UNIVERSITY OF OKLAHOMA

GRADUATE COLLAGE

SUSTAINABLE 3D PRINTED COMPOSITES WITH TUNABLE PROPERTIES AND FUNCTIONAL MICROSTRUCTURES

A DISSERTATION

SUBMITTED TO THE GRADUATE FACULTY

in partial fulfillment of the requirements for the

Degree of

Doctor of Philosophy

By

MD NURUL ISLAM

Norman, Oklahoma

2024

SUSTAINABLE 3D PRINTED COMPOSITES WITH TUNABLE PROPERTIES AND FUNCTIONAL MICROSTRUCTURES

A DISSERTATION APPROVED FOR THE

SCHOOL OF AEROSPACE AND MECHANICAL ENGINEERING

BY THE COMMITTEE CONSISTING OF

Dr. Yijie Jiang, Chair

Dr. Jie Gao

Dr. Jivtesh Garg

Dr. Yingtao Liu

Dedicated to

my parents, the architects of my life

&

my lovely son (Mehmed), the inspiration of my life.

ACKNOWLEDGEMENTS

Throughout my doctoral journey, I've been incredibly fortunate to receive boundless support from numerous individuals who have enriched my path with joy and motivation. First and foremost, I express my deepest gratitude to my academic guru, ***Dr. Yijie Jiang***, whose influence has positively transformed my life in myriad ways. ***Yijie***, thank you for entrusting me and providing unwavering guidance and encouragement at every stage of my PhD studies. Under your mentorship, I've developed critical thinking skills and thrived as an independent researcher. Your passion for science, endless curiosity, and kindness towards others have made me your greatest admirer. It's an honor to not only consider you a mentor but also a true role model.

I also extend my heartfelt thanks to my committee members, Dr. Jie Gao, Dr. Jivtesh Garg, and Dr. Yingtao Liu, for their insightful guidance and support during my doctoral research. Prof. Liu, your support during my transition from the University of North Texas to the University of Oklahoma has been invaluable. Thank you for navigating me through the complexities of grad school policies and ensuring I met all deadlines.

Furthermore, I gratefully acknowledge my mentors from the University of North Texas: Dr. Wonbong Choi, Dr. Sheldon Q. Shi, Dr. Hector R. Siller, and Dr. Nandika D'Souza. ***Prof. Choi***, your meticulous scientific approach and constructive feedback on the piezoelectric sensor project have honed my skills in critically evaluating scientific work. Dr. Shi, Dr. Lee, and Dr. Fu, thank you for your collaboration and discussions on the food-based biodegradable composite with multiscale porosity project. Special thanks to Lee for welcoming me into your lab with warmth and kindness; you are one of the nicest individuals I have ever had the pleasure of meeting.

I extend my heartfelt thanks to all my friends who supported me with their helpful suggestions, mental support, and invaluable friendship during the early days of my PhD journey: Nava, Amoko, Dr. Sanket, Taha, Farhad, Dr. Dipon, Rifat, Siam, Dr. Khorrom, Dr. Utpol, Dr. Hossain, Dr. Jashim, Mahan, Sakib and Aditi. To my cohorts from the past and present members of the Yijie and Choi's research groups: Rifat, Dr. Pashupati, Dr. Azam, Mehrab, Mehrzad, Sanzida, Sophia, Guanying, Gary, Ravi, Thu, Sreerjit, Hojae, and Alejandro, thank you all for sharing this incredible journey with me.

Lastly, to my lovely wife, ***Fatima***, thank you for your unconditional love and unwavering encouragement that have propelled me towards achieving my goals. Without your support, I wouldn't have been able to even write this dissertation. I'm deeply grateful to my parents for their sacrifices that have shaped me into who I am today. ***Ma***, your resilience has taught me how to navigate through challenging times, and ***Baba***, thank you for instilling in me the importance of always doing the right thing. I also want to express my heartfelt gratitude to my elder brother, ***Arif***, for holding our family together all these years. You're my role model, and I love you dearly.

Table of Contents

List of Figures

List of Tables

Abstract

The environmental impact of petroleum-based plastics has prompted the search for eco-friendly alternatives. Nature-based sustainable materials emerge as compelling substitutes, given their abundance, renewability, biocompatibility, and biodegradability, effectively addressing both environmental and health risks associated with petroleum-based plastics. Recent advances in green biocomposites from plant-derived fiber and crop-derived matrix have stimulated interests in developing engineering-grade and multifunctional materials for additive manufacturing (AM). Direct ink writing (DIW) is an AM technique that enables the customized and precision fabrication of composites with enhanced mechanical properties through microstructural control.

This dissertation focuses on developing 3D printable, recyclable, biodegradable, and functional advanced composites to mitigate the environmental and health hazards linked with petroleum-based plastics. The composite material is derived from amylopectin-rich corn starch and cellulose fibers sourced from corn products and waste. We leveraged a thermally activated gelatinization process of amylopectin molecules to achieve optimal rheological properties of the corn-based composite for 3D printability in DIW. The process utilized the thermal treatment effect on hydrogen bonding formation among amylopectin molecules as well as between amylopectin and cellulose fibers interfaces, thereby enhancing mechanical robustness. The process-structure-property relationships revealed tunable mechanical properties up to 3.3-fold in the printed specimens. Furthermore, recyclability tests demonstrated stable mechanical performance of the 3D printed specimens over 10 cycles compared to pristine samples.

Additionally, we introduced a process-microstructure guided manufacturing approach for fabricating three-dimensional porous structures with hierarchical porosity for application in emerging fields like tissue engineering, bone scaffold, and drug delivery due to their distinctive

porosity-driven functional properties. By harnessing the degree of amylopectin gelatinization coupled with 3D printing, we attained precise control over pore size at multiple length scales (macro, micro, and nano). Macropores are engineered via printing path design, while degree of gelatinization governs micro and nanopores formation. process-microstructure relationships demonstrated up to 2.3-fold control over micropores and over 3-fold for nanopores. The novel approaches reported in this dissertation offer opportunities to achieve tailored porosity at macro, micro, and nano scales within composite microstructure. These composites, derived solely from biomass and waste, represent a novel class of additively manufacturable sustainable materials that underscore the potential for replacing petroleum-based plastic, marking a significant stride towards sustainable manufacturing practices. With the rising demand for eco-friendly solutions, these natural material-based composites offer compelling alternatives with diverse applications across advanced engineering and biomedical fields.

Chapter 1: Introduction

1.1 Motivation: Petroleum-derived plastics that are lightweight, low-cost, and durable find a wide range of applications in construction, automobiles, aviation, electronic, packaging, and biomedical implants. However, most plastics take hundreds of years to degrade due to extremely low degradation rates[1,2]. Therefore, both the raw materials used to make them and their disposal after their service life pose environmental concerns[1–3]. Besides, petroleum-based composite recycling faces key challenges, such as the difficulty of separating fiber and matrix from their structures to allow for recycling after service life[4]. As a result, only 18% of plastics are recyclable, with the real recycling rate being 6 to 8.4%, even though 400 million tons of plastic waste are produced every year[5–7]. Furthermore, recycling petroleum-based plastics faces numerous obstacles, including the use of heavy chemicals, energy, and complex manufacturing processes associated with high costs[8] which further pollute the environment. Additionally, studies indicate that the mechanical properties of recycled petroleum-based materials degrade over recycling cycles, further exacerbating sustainability challenges[9]. To mitigate these issues, researchers advocate for the integration of cellulose fibers sourced from biobased materials like jute, corn, cotton, and sisal into composite materials, aiming for enhanced sustainability. They have proposed chemical crosslinking or surface modification of the filler to improve interfacial interaction between filler and matrix into composite microstructure to boot the overall mechanical properties of the composite materials. However, these approaches still aren't sustainable as they require the use of chemicals and can't get rid of the recycling complexities. Furthermore, the incorporation of bio-based fillers with petroleum-based plastics fails to address sustainability concerns, as petroleum-based materials still dominate the composite.

To address the environmental and health concerns linked to heavy reliance on petroleum-

based plastics, emerging researchers endeavor to develop fully sustainable high-performance structural materials that are biodegradable, easy to recycle with minimal processing cost and use of chemical, and more environmentally friendly using sustainable materials[10–16]. Nonetheless, challenges persist, as bio-based materials and their composites often exhibit limited mechanical properties and necessitate chemical intervention and high manufacturing expenses. Microstructural modifications play a crucial role in enhancing the mechanical properties of bio-based composites, highlighting the significance of advanced strategies in material design and manufacturing. Therefore, it is of great importance to introduce an advanced strategy to design & manufacture sustainable high-performance structural materials. Additive manufacturing, also known as 3D printing, emerges as a promising avenue for enhancing the properties of natural materials via microstructure control. Researchers are increasingly leveraging additive manufacturing techniques, such as fused deposition modeling (FDM) and direct ink write (DIW), to develop sustainable composites using bioderived materials[17,18,11,19–22]. These advancements enable the production of bio resource sustainable composites and facilitate property improvements through microstructure control[11,17–20,23,24]. For example, *Estakhrianhaghighi et al*. developed sustainable materials for low cost additive manufacturing using bio-based polymer and cellulose fibers from waste wood[17]. They made 3D printable filament for FDM and were able to enhance its stiffness, ultimate strength, fracture strain, toughness and thermal conductivity compared with the PLA counterpart. *Jiang et al.* demonstrated the power of DIW 3D printing for controlling fiber orientation, distribution, and alignment within the matrix to enable precisely program the composite microstructure and enhance its mechanical properties. They formulated 3D printable composite materials using sticky rice and cotton fibers for direct ink writing 3D printing technique and the resulted composite showed comparable stiffness and was more resistant to fire and

degradation compared to PLA-wood composite[11]. Despite these advancements, challenges persist in achieving desired mechanical stiffness in 3D printed natural materials. To address this, researchers have explored the incorporation of synthetic materials and hazardous chemicals, compromising sustainability objectives.

Natural materials, such as protein, lignin, and starch, have been investigated as matrix materials in DIW 3D printing[11,22,29]. Among these resources, corn has the largest market with global production exceeding 1.2 billion metric tons and US is the largest corn producer with an estimated production volume of 384 million metric tons in 2021/2022[30,31]. Deriving from corn biomass, starch has its advantages due to its biodegradability, origin from food and abundance in nature[12,17,32–35]. However, starch-based composites are typically not designed for load-bearing application[22,29]. For example, 3D printed corn starch has low stiffness and mostly is used as a temporary sacrificial material[22,29]. Cellulose fibers have been used with synthetic polymer as the reinforcement[12] due to their superior mechanical properties[19]. However, the hydrophilic character of cellulose fibers is incompatible with synthetic hydrophobic polymers, leading to poor interfacial bonding between fillers and matrix[14,36]. In contrast, reinforcing corn starch matrix with cellulose fibers may improve filler-matrix compatibility since both fibers and matrix are hydrophilic[11,21]. Such compatibility might strengthen the fiber-matrix interface and contributes significantly to the composite's mechanical properties[21,36]. Although there are emerging researches using natural materials into 3D printing[11], mechanically robust and printable materials using neat natural resources are limited, and the fundamental process-structure-property relationships to guide manufacturing, structural design, and properties tuning are not fully established.

1.2 Objectives: The overreaching objective of this dissertation is to develop 3D printable, recyclable, biodegradable, and functional advanced composite, focusing on corn-based materials.

The study introduces a thermally activated gelatinization process for amylopectin molecules to enhance mechanical properties and achieve multiscale porosity in 3D printed corn-based composites. This work includes the following sub-objectives:

- **Aim 1** focuses on the development of a 3D printable composite via a thermally activated gelatinization process of amylopectin molecules and signifying the role rheology in DIW 3D printing for 3D structure fabrication.
- **Aim 2** investigates the thermo-mechanical effects on mechanical characterization, exploring the dependency of material properties on material microstructure.
- **Aim 3** targets to achieve tunable porous structures through the integration of thermomechanical treatment with 3D printing, offering composite microstructure customization possibilities for diverse applications.
- **Aim 4** investigates the recyclability of the 3D printed corn-based composites, ensuring a closed-loop approach to material usage for circular economy.

1.3 Scope: The reported composite material in this dissertation is derived from amylopectin-rich corn starch and cellulose fibers sourced from corn products and waste. Understanding thermally activated gelatinization process of amylopectin molecules to achieve optimal rheological properties of the corn-based composite for 3D printability in DIW and tuning hydrogen bonding formation among amylopectin molecules as well as between amylopectin and cellulose fibers interfaces, for controlling microstructure and enhancing mechanical robustness. The scope of this dissertation is described below. Firstly, a review of the relevant literature on additive manufacturing, sustainable materials, material recycling for sustainability and functionalities in sustainable materials and their applications is presented in Chapter 2. Next, chapter 3 introduces a two-step hybrid cellulose fibers extraction method from corn husks with tailored dimensions,

suitable for smooth 3D printing. Those fiber act as reinforcement into corn starch to enhance its mechanical properties. Then a thermally activated process of amylopectin molecules is introduced to achieve desirable level rheological properties of the corn-based composite for 3D printability in DIW. Rheological measurements as a function of shear yielding and thinning properties are introduced first. Afterward, printability mapping of the printable inks with water concentration and critical yield stress is demonstrated. Later, ink aging impact on both rheology and 3D printability is examined to show how these factors evolve with the ink's pot life. Chapter 4 investigates the thermo-mechanical effect on mechanical characterization in the 3D printed corn-based composites. Our exploration begins with a study on how the choice of filler, filler fraction and density of the 3D printed specimen impacts the overall mechanical properties of the starch matrix. Following these investigations, we introduce a novel method for thermally strengthening 3D printed corn-based composites through a process that integrates thermal treatment of the amylopectin molecules coupled with Direct Ink Writing (DIW) 3D printing. This innovative approach allows for precise control over the microstructure of composites, thereby enhancing their mechanical robustness. The investigation of the thermo-mechanical effect on microstructure characterization in the 3D printed corn-based composites is described in Chapter 5. We have introduced a process-microstructure guided manufacturing route for fabricating three-dimensional porous structures with hierarchical porosity. By harnessing the thermally activated gelatinization process of amylopectin molecules coupled with 3D printing, we have unlocked the mechanism to achieve precise control over pore size across multiple length scales. This approach yielded substantial tunability in macro, micro, and nano pores within the printed composites. Chapter 6 presents the mechanical and microstructural properties of the recycled 3D printed composite. The recyclability tests of the 3D printed specimens are conducted over 10 cycles.

1.4 Societal impact: The global 3D printing market for plastic-based materials used in melt extrusion-based printing is dominated by petroleum-based thermoplastics. PLA based 3D printing filament market was estimated at $2 billion in 2023 and is projected to grow $15 billion by 2036[100]. Despite the benefits that nature-based materials offer for additive manufacturing, the market remains limited. Taking advantage of the pure corn-based materials, which are renewable, biodegradable, low cost, and its advanced properties such as 3D printability, thermally strengthening behavior, and programable porosity, the reported composites may mitigate the global challenges posed by high-volume utilization of petroleum-based plastics and can create additional revenue streams for biomass processing industries.

Chapter 2: Literature Review

2.1 Additive manufacturing (AM): Patterning materials in three-dimensional space is critical in emerging applications, including microfluidics[28], photonics[28], tissue engineering[29], drug delivery[22,37,38], lightweight engineering materials[11], wearable electronics[28,39], sensors[40], batteries[41,42], fiber composites[11,26] and shape morphing designs[43], and many others. AM also known as 3D printing has gained significant interest owing to its ability to fabricate three-dimensional object and drive technological development for customizable and precise structural designs, as well as low waste and fast fabrication[44,45]. The global 3D printing market size is expected to reach around $ 76.17 billion by 2030.

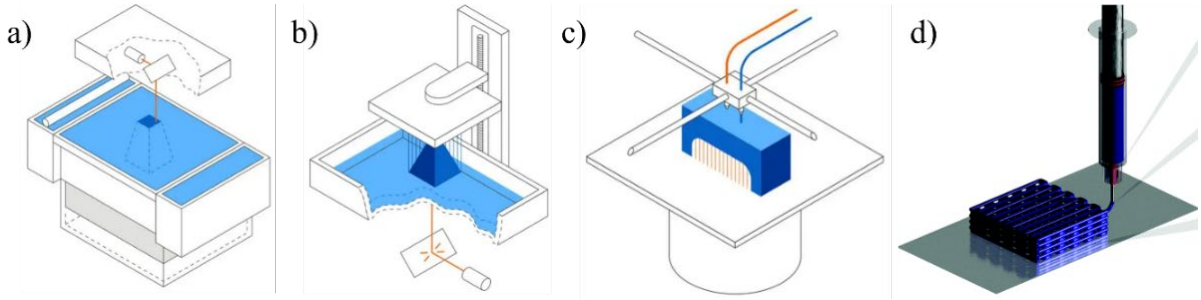

Figure 2.1: Additive manufacturing methods: a) Selective laser sintering (SLS), b) Stereolithography (SLA), c) Fused deposition modeling (FDM) and d) Direct ink writing (DIW)[101, 102].

So far, AM can be categorized into 7 types, including vat photopolymerization, material jetting, binder jetting, material extrusion, powder bed fusion, sheet lamination and directed energy deposition[46]. Among them, several 3D printing methods are becoming widely used in research and industrial fields, such as FDM[18], DIW[26,28,47], stereolithography (SLA)[48], and selective laser sintering (SLS)[49] (Figure 2-1). Each method has its own printable material selections[27]. FDM, for instance, is suited for printing thermoplastic polymers, SLA can print photocurable materials, and SLS is suitable for printing metals, alloys, and ceramics[27].

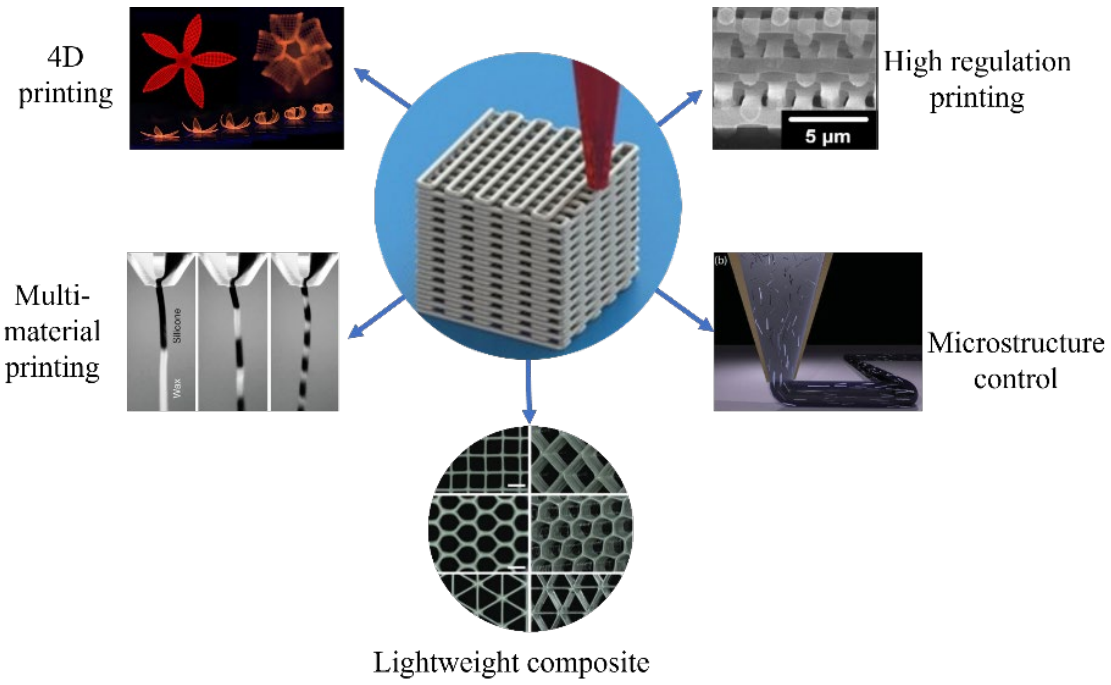

Figure 2.2: Applications of DIW 3D printing method for functional devise and structure fabrication[26,28,43,51].

DIW printing is distinct from other AM technologies due to its advantages in a wide range of printable materials and minimal requirement of printing environment[27]. The materials can be effectively printed into a 3D structure with intended material properties as long as their exhibit desired rheological properties, specifically shear thinning and yielding behavior under shear[26,28,47]. In addition to the freedom of materials choice, DIW technique is capable to integrate active and passive controls mechanism with 3D printing system to control the microstructure of the printed structure[11,25–27,50] (Figure 2-2). In an active approach[27], magnetic fields, electromagnetic waves, acoustic waves, and heat sources are inserted, while in a passive approach[50], helicoid channels are integrated into materials holding syringe. DIW's versatility is further enhanced by the ability to fabricate multi-material structures through the extrusion of multiple materials into a single design[51,52](Figure 2-2). It also provides a promising technology for fabricating shape-morphing structure using smart materials that respond to external stimuli through 4D printing[43,53](Figure

2-2). In addition to product design and prototyping, this AM method has potential to manufacture products on an industrial scale[11,21,26]. Thus, DIW has emerged as a powerful manufacturing process for emerging technologies in composite manufacturing, organ printing, tissue engineering, food printing, soft robotics, electronics, sensors, energy storage and harvesting.

Figure 2.3: Fibers and fillers from renewable and sustainable resources for sustainable composite materials[21,103,104,105,106,107,108].

2.2 Sustainable materials: Bio composites, comprising of a nature based biodegradable polymer as the matrix and biofiber as the reinforcement, inherently possess biodegradability and environmental friendliness due to the biodegradable nature of both components (Figure 2-3). In contrast, petroleum-based plastics, derived from synthetic polymers, lack biodegradability. Composites incorporating natural fibers and non-biodegradable synthetic polymers represent a novel material class but do not achieve complete biodegradability. Heightened global environmental consciousness has spurred a shift towards designing materials that align with

environmental sustainability. Biofibers sourced from natural resources, serving as reinforcing fibers in both thermoplastic and thermoset matrix composites, offer notable environmental advantages over petroleum-based materials (Figure 2-3). There is growing interest in developing nature-based advanced and functional materials for AM as they are renewable, recyclable, biodegradable and environmentally friendly replacements for currently used petroleum based-materials[8,11,12,17,19,21–23,54–56] (Figure 2-3). For example, *Nguyen et al.* reported the manufacturing of high-performance class of printable materials for FDM using lignin, a biomass feedstock[18] (Figure 2-4a). Since materials' rheology plays a key role in extrusion-based AM, they optimized lignin's viscosity with nylon and carbon fiber for good printability. In addition to viscosity tunability, carbon fibers improve mechanical and thermal properties, making them ideal for unidirectional heat transfer and directionally reinforced structures applications. Their approach allows lignin to be used as a renewable feedstock for 3D printing applications. Due to its thermoplastic nylon content, however, the reported composite material is not entirely biodegradable. *Akbarzadeh et al.* developed completely biodegradable materials for FDM using biodegradable PLA and cellulose fibers[17] and printed the composites into architected cellular structures for characterization. The printed materials exhibited improved mechanical and thermal properties compared with their PLA counterpart. They harnessed the unique property of extrusion-based AM methods to control the fiber distribution, and alignment into the matrix to make composite stiffer, stronger, and tougher. Despite the fact that FDM is the most affordable additive manufacturing technology, filament fabrication is a complex and time-consuming process, and it has constraints in printing resolution, quality, and material selections limit within thermoplastics[27]. In contrast, ink can be printed in 3D structure with high-resolution patterning using DIW[19,27]. For example, *Pattinson et al.* exhibited the versatility of the DIW by printing fully dense cellulose-

based materials and demonstrated the potential of cellulose as an abundant, renewable, recyclable, biodegradable and chemically versatile material for AM[19](Figure 2-4d). Using a 200-micron (um) nozzle, they printed miniature eyeglass frames and small roses with smooth surface finishes to demonstrate how small features can be reproduced with smaller nozzles and reported that a lot of smaller details could also be regenerated. In addition to making mechanically robust objects, they tailored cellulose-based materials with biochemical functionality and demonstrated its antimicrobial properties in customized medical instruments.

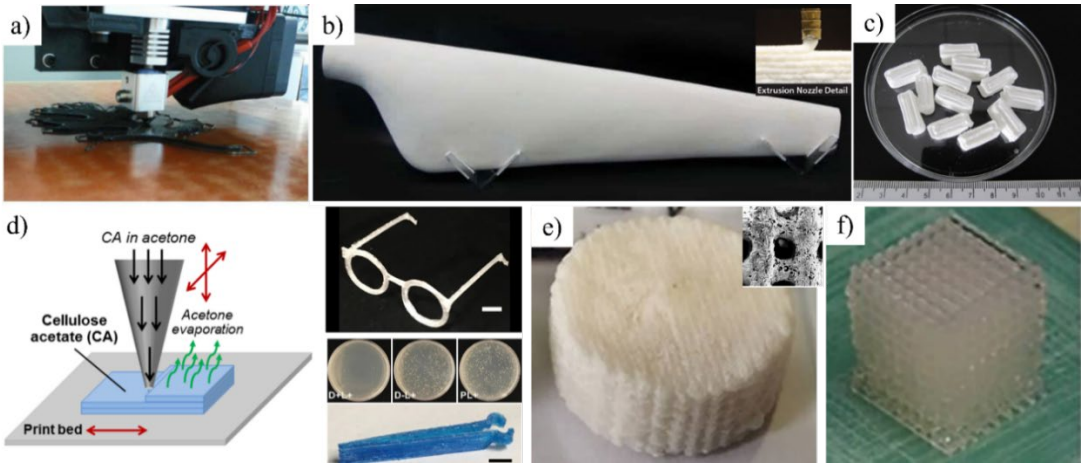

Figure 2.4: Additive manufacturing of biobased materials for a) wood printing, b) large scale structure of wind turbine blade, c) capsule for drug delivery, d) antibacterial structure and e-f) cellular scaffold for bone tissue regeneration application[19,20,22,37].

Since scalability is one of the biggest challenges in AM, *Sanandiya et al.* addressed the scalable aspect of DIW by printing large 3D objects using cellulose based materials[20](Figure 2-4b). They fabricated a 1.2 m long lightweight and mechanically robust wind turbine blade. Besides mechanical applications, the 3D printed natural materials can have medical functionality. *Khaled et al.* for example demonstrated how 3D printing can be used to tailor medicine manufacturing for personalized care[22,38](Figure 2-4c). They used extrusion-based 3D printing to manufacture the multi-compartment tablets each with a well-defined controlled drug release profile to deliver

multiple active ingredients. To deliver drugs in specific environments, they programmed tablets with two different drug release mechanisms: diffusion through gel layers and osmotic release through a controlled porosity shell (Figure 2-4e-f). They have made a significant contribution to the development of tailored manufacturing of medicines for personalized care and treatment using 3D printing.

2.3 Material recycling for sustainability: Materials recycling plays a crucial role in sustainable development, circular economy to minimize and eventually remove material waste from the system, and combating the use of petroleum-based materials[4,14,15]. Besides, recycling petroleum-based materials are highly challenging, such as the difficulty in disintegrating the fibers and matrix from the composite structures[4]. Furthermore, recycling them requires a considerable amount of chemicals, energy, and high manufacturing costs due to their complex manufacturing process. The material itself can even degrade over time through repeated recycling[4]. In contrast, nature-based composite materials are easy to recycle and require less processing since fiber and matrix don't need to be separated and recycled composites sometime outperform their virgin counterparts[57,58]. Wood and other natural fibers such as corn, cotton, jute, flax and sisal can be used to reinforce petroleum-based plastic for biocomposite materials (Figure 2-3). *Bodur et al.* recycled cotton fibers reinforced low density polyethylene (LDPE) composite. After recycling, the composites' tensile strength and Young's modulus first increased and then decreased[57]. Meanwhile, the tensile strength of the neat LDPE sample decreased with recycling, suggesting degradation of polymer and chain scission. They attributed the initial increase in the tensile performance of the composites to the increased aspect ratio of the cotton fibers and a better-quality dispersion upon recycling. Several studies have seen similar increase tensile properties and subsequent decrease during repeated reprocessing of wood fiber reinforced thermoplastic

matrix[58,59]. Although natural fiber reinforced polymer composites (NFRPC) are often regarded as green, sustainable, and recyclable materials, they are not entirely derived from renewable resources[14,18]. While the renewable and sustainable resource-based biocomposites bio-composite simultaneously benefits from the recyclability and biodegradability of wood and biopolymers[8]. *Xia et al.* reported an *in-situ* lignin regeneration approach to manufacturing strong, scalable, biodegradable, and recyclable lignocellulosic bio-composite using lignin and cellulose fibers[8]. Using lignin as a natural glue, the micro/nanofibrils of cellulose are tightly wrapped and linked together, forming a homogenous slurry with high solid content. Furthermore, strong hydrogen bonding interactions between lignin and cellulose enhance its mechanical properties. The resulting composite material demonstrates high tensile strength, excellent water stability, and improved thermal stability. More importantly, reported material is biodegradable by natural microorganisms and recyclable by simple mechanical disintegration and resulted in much lower environmental impacts than petrochemical-based plastics.

2.4 Functionalities in sustainable materials and their applications: Porous biomaterials are receiving significant interest in biomedical applications, including bone tissue regeneration[29,60–64], drug delivery[37,38,60,62,63,65,66], microfluidic devices[67,68] and hemostatic[66,69] due to their intrinsic properties of biodegradability, non-toxicity, origin from food, abundance in nature, and, more importantly, being able to be biocompatible. Porosity is one of the key material features to mimic the extracellular matrix of the human tissue in designing functional and biocompatible tissue scaffolds[29,60,61,66,70], drug delivery systems[37,38,65] and microfluidic device[67,68]. The presence of pores in the scaffold enables oxygen and nutrient exchange, cell migration, and waste product expulsion in bone regeneration application[63,64]. Previous studies reported that porosity, pore size, and pore interconnectivity play crucial roles in repairing bone tissue defects as they provide the

adequate surface area in the scaffold to enhance cells and the surrounding tissue interaction[29,63,64]. Larger pores promote cell proliferation and growth while small spaces lead to cell differentiation[63,64]. Optimum pore size and interconnectivity for effective bone tissue formation are in the range of 100–400 μm and 30–90%[64]. In drug delivery, voids are typically intended to be saturated with biological fluids, thereby enabling drug release through material degradation or outward drug diffusion[37,63]. Surface-to-volume ratios of materials are also affected by porosity, and larger surface-to-volume ratios can provide greater access for cell attachment for bone reconstruction as well as increase the pharmaceutical agent release rate in drug delivery applications[63]. Microfluidic devices, on the other hand, rely on capillary action mechanisms to guide fluids through pores[67]. This is due to the pore size and surface tension of the fluid with the material walls. Apart from biomedical application, porous biomaterials are being used in energy harvesting and storage[71] applications to fabricate sensor[62,71,72], supercapacitor[62,73] and batteries[62,72]. High specific surface area and controllable porosity motivated emerging researchers to use starch for hierarchical porous carbon for high performance supercapacitors[73]. In such hierarchical structures, the abundant micro- and mesopores provide a high accessible surface area and play an essential role in high energy storage resulting in a large capacitance and high energy density, while the interconnected meso- and macropores facilitate the fast ion transport by supplying ion-buffering reservoirs and ion-transport pathways, which ensure the high-rate capability and high-power density.

Chapter 3: 3D Printable Ink Formulation Mechanism

3.1 Chapter Introduction: 3D printing enables the fabrication of 3D structures with arbitrary geometry. Direct ink writing has emerged as a simple yet effective manufacturing method for fabricating customizable and precise composite structures, offering several distinct advantages such as (i) compatibility with a wide array of printable materials, (ii) minimal printing environment requirement and (iii) functionalities to enhance the mechanical properties through precise control over microstructure. In the DIW process, viscoelastic inks are extruded from a translating nozzle under shear stress and fabricate 3D object in a layer-by-layer deposition of material. To ensure successful fabrication, the entire process can be sub divided into three essential steps: (i) ensuring smooth flow through the syringe and nozzle, (ii) achieving continuous ejection of the ink from the nozzle, and (iii) ensuring smooth deposition of the ink on the printing platform. Consequently, the 3D printable inks used in this method must meet stringent criteria for 3D printability, typically defined in terms of rheological properties. These properties encompass shear yielding, characterized by the transition of starch-based materials from a gel-like to a fluid-like response, and shear thinning properties, characterized by the smooth flow of the ink under shear rate. Therefore, the rheological properties of the inks determine which materials are suitable for 3D printing via direct DIW.

This chapter introduces a sustainable manufacturing route to formulate 3D printable inks entirely from corn-based materials and waste. The composites are made by amylopectin in corn starch and hybrid cellulose fibers, which are extracted from corn husks through a two-step chemical process. We leverage a thermally activated gelatinization process of amylopectin molecules to turn corn starch into viscoelastic materials, suitable for DIW. The rheological properties of these inks are tailored through water content and filler fraction, resulting in

composites that exhibit shear yielding and shear thinning behavior.

3.2 Materials and Methods: The composites are made from amylopectin-rich corn starch and cellulose fibers derived from agricultural waste.

3.2.1 *Amylopectin:* Corn starch is a complex mixture comprising both amylose and amylopectin structures (refer to Figure 3-1a). Amylose features relatively short and linear α-1,4 linked glucose units. On the other hand, amylopectin is a high molecular weight natural biopolymer with highly branched structures. The amylopectin is a polysaccharide consisting of a backbone of alpha-1,6 bonds as main chain and short α -1,4 side chains (~5 nm) [35,74,75]. These side chains form a helicoidal structure, as depicted in Figure 3-1b. For this study, we employ a corn starch variant rich in amylopectin (amylopectin: amylose ≈ 100:0), specifically Waxy Maize from Now Sports. When amylopectin is heated with water, starch granules undergo gelatinization, during which the side branches open to form a large network as gel balls (as shown in Figure 3-1b). This process exposes -OH and -COOH functional groups, which can potentially engage in hydrogen bonding with amylopectin granules and other surfaces rich in hydrogen bonds, such as cellulose fibers.

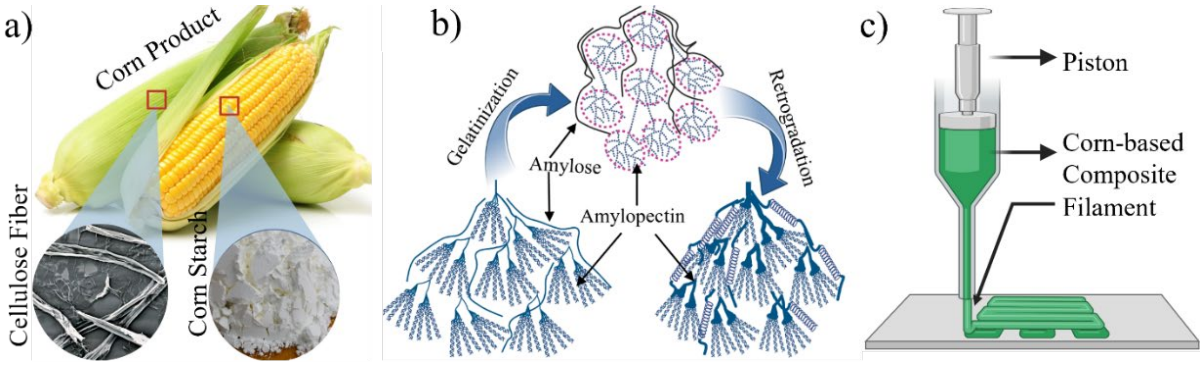

Figure 3.1: a) Corn starch and cellulose fiber from corn. b) Schematic representation of phase transition for starch during gelatinization and retrogradation. c) Direct ink writing 3D printing.

3.2.2 *Cellulose fibers*: Natural fibers consist mainly of cellulose, hemicellulose, and lignin, with minor amounts of wax, pectin, and sugars. Where cellulose is the stiffest and strongest organic

component, providing the fiber with strength, stiffness, and stability[76]. In cellulose, glucose units are linked together in long chains, which are further organized into bundles known as microfibrils[76]. The cellulose fibers used in this study were extracted from corn husks through a multi-step mechanical and chemical process.

3.2.3 *Extraction of cellulose fiber:* We extracted hybrid cellulose fibers from corn husk through two step chemical treatment. At first, corn husks (sourced from Los Chileros, USA) were dried in an oven at 100ºC for 2 hours to remove moisture. Following drying, the corn husks were chopped into small pieces (as illustrated in Figure 3-2a) and then processed through a grinder (2.6 HP Table Type Ultra Fine Powder Pulverizing Machine, RT-UF26). The resulting powders were subsequently sieved using a 300-micron fine mesh (Figure 2b), and these powdered corn husks were referred to as "raw fiber" (RF), which includes cellulose, hemicellulose, and lignin[77–79]. Hemicellulose and lignin were selectively removed through a two-step chemical treatment process [80–82] as shown in Figure 3-2c. In the alkalization step, an alkali solution was prepared by dissolving 50 g of sodium hydroxide (NaOH, Sigma-Aldrich) in 1250 ml of DI water. Then the 2 wt% powdered corn husks soaked into the alkali solution, heated on a hot plate, and stirred by a magnetic stirrer (Firstaden Lab) at 200 rpm for 4 hours at 80ºC. The resultant solution was thoroughly washed with DI water to achieve a pH of 7. The suspension was then centrifuged (Ohaus FC5706) at 2000 rpm for 10 minutes and dried in ambient conditions. Afterwards, alkali treated fibers were delignified by a solution made of 4% (w/v) sodium chloride (NaCl, Milipore-Sigma) and 4% (v/v) acetic acid (CH_3COOH, Milipore-Sigma) in 625 ml DI water. Then the delignified suspension was mixed by a magnetic stirrer at 200 rpm for 24 hours at 30ºC. After delignification, the resultant solution was washed thoroughly with DI water until pH became 7. After being washed thoroughly, cellulose fibers (CF) were centrifuged (Ohaus FC5706) at 2000

rpm for 10 minutes and dried in a freeze dryer (Harvest Right, HRFD-Med-SCI).

3.2.4 *Printable ink formulation:* Inks were formulated as a mixture of corn starch (amylopectin, Waxy Maize, Now Sports®), cellulose fibers, and water. The corn starch and water first mixed with the ratio given in Table 1 at 1800 rpm for 3 minutes under vacuum using a mixer (Flacktek®, DAC 400.2 VAC). Then thermal treatments of the inks were carried out in a drying oven (Huanghua Faithful Instrument Co., LTD) at 120ºC for 6, 8, 10, 12, and 14 minutes, respectively. This preheating treatment led to the gelatinization of amylopectin, i.e. the helix side chains expanded into gel balls and exposing hydrogen bond positions[11,35,74,75] (Figure 3-1b) After heating, 10wt% of cellulose fibers were added into the gelatinized corn starch in the ratio shown in Table 1. Finally, the composites were mixed at 2000 rpm for 2 min and 1500 rpm for 2 min in the mixer. We also developed inks with different cellulose fiber loading as shown in Table 2 with preheating temperature of 120ºC for 10 minutes.

Table 1: Ink formula as a function of preheating condition for CS-CF10 ink.

Preheating time (min)	***Corn Starch, (g)***	***Water (g)***	***Cellulose Fiber, (g)***
6	6	7	0.63
8		7.5	
10		8	
12		9	
14		9.5	

Table 2: Ink formula with fiber fractions at thermal treatment of 100ºC preheating for 10 min.

Ink Type	***Corn Starch, (g)***	***Water (g)***	***Cellulose Fiber, (g)***
CS	6	7.5	0
CS-CF5		7.5	0.315
CS-CF10		8	0.63
CS-CF15		9.5	0.945
CS-CF20		10	1.26

3.2.5 *Ink Rheology Charecterization:* Rheological characterizations of the pure corn starch ink, the inks with 10 and 20wt% cellulose fibers were measured using a rotational rheometer (MCR 72, Anton Paar®) with 24.9 mm diameter flat plates and a gap of 1 mm. Storage and loss modulus were measured as a function of shear stress and viscosity was measured with a ramp logarithmic shear rate of 0.01–100 s^{-1}. All rheological measurements were conducted at 25°C with 1 minute preconditioning.

3.2.6 *3D Printing:* Corn-based composites were 3D printed using a custom-built DIW 3D printer, consisting of a dispensing unit (Ultra TM 2800, Nordson EFD®) and MakerGear® M2 printer. Multi-layered triangular structures and bulk bending specimens were printed with customized G-code. Inks were loaded into a 10cc syringe (Nordson EFD®) and centrifuged (Ohaus® FC5706) for 3 minutes at 2500 rpm to remove air bubbles. Afterwards, syringe was sealed with a piston and a 610 µm nozzle (Nordson EFD®) was connected with a Luer lock in extrusion. Then the syringe was mounted in the custom-built DIW 3D printer. All specimens were printed with the following printing conditions, 0.003 cc/sec material extrusion rate, 10 mm/sec printing speed, and an experimentally determined layer height of 400 µm. Moreover, composite inks can be printed at a printing speed of 5-40 mm/s and extrusion rate 0.0015-0.012 cc/s, varying linearly proportional to the printing speed using a 0.61 mm nozzle. Nozzle size larger or equal than 0.61 mm can be used for printing without clogging.

3.2.7 *Aging effect on composite rheology and 3D printability:* Ink aging effect was investigated on both rheology and 3D printability. After inks formulation, they were sealed and stored in a refrigerator at (-20°C). After the aging process, inks were activated by heating in a drying oven (Huanghua Faithful Instrument Co., LTD) for 10 minutes. Then the activated inks were employed for comprehensive rheological measurements and subsequently utilized in 3D printing to produce

specimens for subsequent microstructural and mechanical assessments. The mechanical properties and structural evolution were systematically recorded over a defined pot life period, extending up to 120 days, to assess the aging effect on the composite material.

3.3 Results and Discussion:

3.3.1 *Cellulose Fiber Characterization:* Hybrid cellulose fibers were extracted from corn husks, tailored to have dimensions suitable for smooth 3D printing to fabricate controllable 3D structure. The initial raw fiber (RF) composition comprised primarily cellulose, hemicellulose, and lignin, with cellulose imparting robust mechanical properties to the resulting composites [77–79]. Therefore, to maximize these composites mechanical robustness, we subjected the raw fiber to a chemical processing step, selectively removing hemicellulose and lignin, effectively isolating cellulose as the dominant fiber component (Figure 3-2c). Fourier Transform Infrared (FTIR) results were acquired for both raw and cellulose fibers, as depicted in Figure 3-2d-e. In the raw fiber (RF), the FTIR spectra revealed pronounced hydrogen-bonded O-H and C-H stretching in the cellulose peaks, evident in the 3000-3600 cm^{-1} and 2800-3000 cm^{-1} ranges, respectively[80,89]. An absorbance peak at 1724 cm^{-1} corresponded to the stretching of the C=O group, indicative of hemicellulose content[80,89] In lignin, sharp peaks at wavenumbers 1630 cm^{-1} and 1513 cm^{-1} were attributed to aromatic rings, while 1233 cm^{-1} corresponded to aryl groups[80,89]. The removal of hemicellulose and lignin from the fibers was evident, as these characteristic peaks (1724, 1630, 1513, and 1233 cm^{-1}) vanished (Figure 3-2e). The extracted cellulose fibers represent a hybrid mixture of micro and nano fibers (Figure 3-2f-g). Individual microfibers can be observed in Figure 3-2f, while nanofibers form a complex network (Figure 3-2g). The size distribution of microfibers and nanofibers is illustrated in Figure 3-2h-j. Microfibers exhibit an average length and width of 64±24 and 9.8±4μm, respectively (Figures 3-2h-i). Nanofibers, on the other hand, possess an average

width of 311±106 nm and an aspect ratio exceeding 95 (Figures 3-2j). Notably, the chemical treatments not only removed hemicellulose and lignin but also reduced the fiber dimensions, rendering the resulting cellulose fibers suitable for seamless 3D printing.

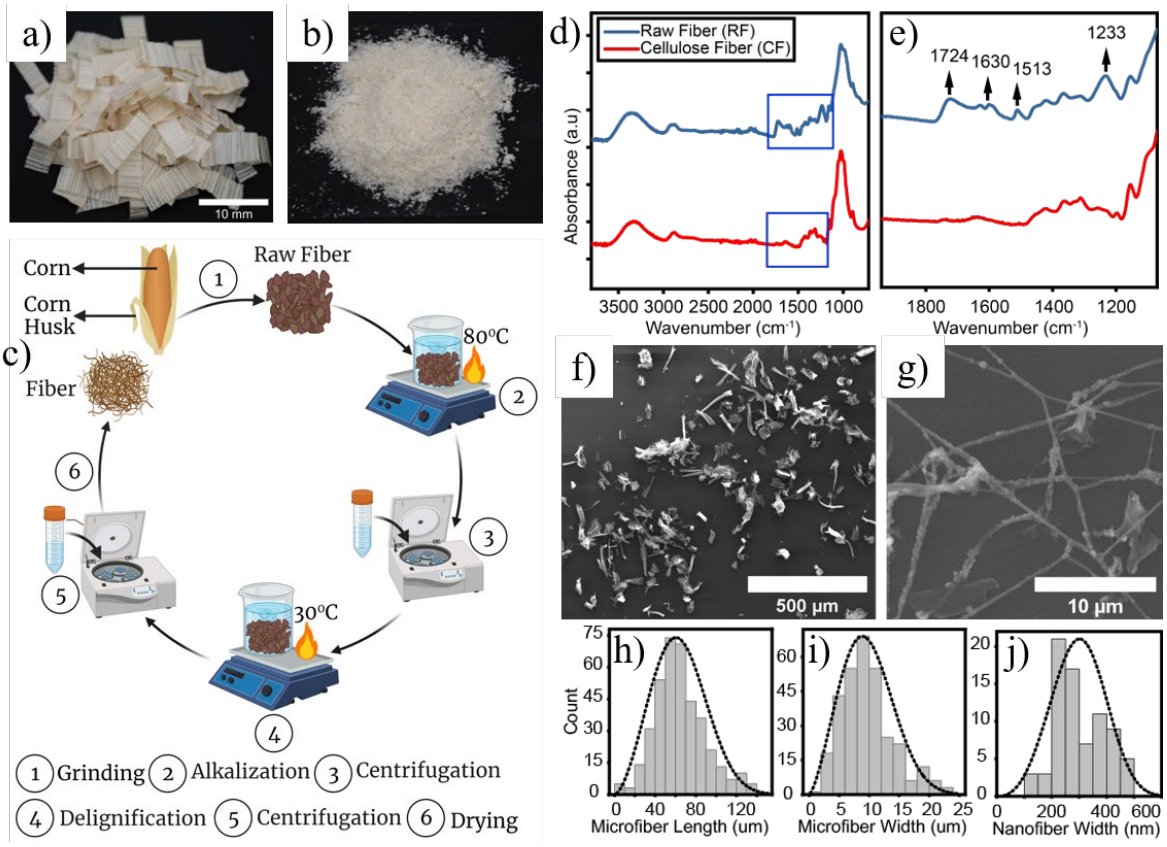

Figure 3.2: Cellulose fibers extraction and characterization. (a) Raw materials of chopped corn husks. (b) Cellulose fibers (CF) extracted from corn husks after mechanical and chemical processes. (c) Schematic of cellulose fibers extraction processes. (d, e) FTIR spectra comparison between raw fibers (RF) before delignification and CF, showing that effective removal of hemicellulose and lignin resulted CF. SEM observation of (f) cellulose microfibers and (g) cellulose nanofibers. Dimensional characterization: (h) length and (i) width distributions of cellulose microfibers and (j) width distribution of cellulose nanofibers.

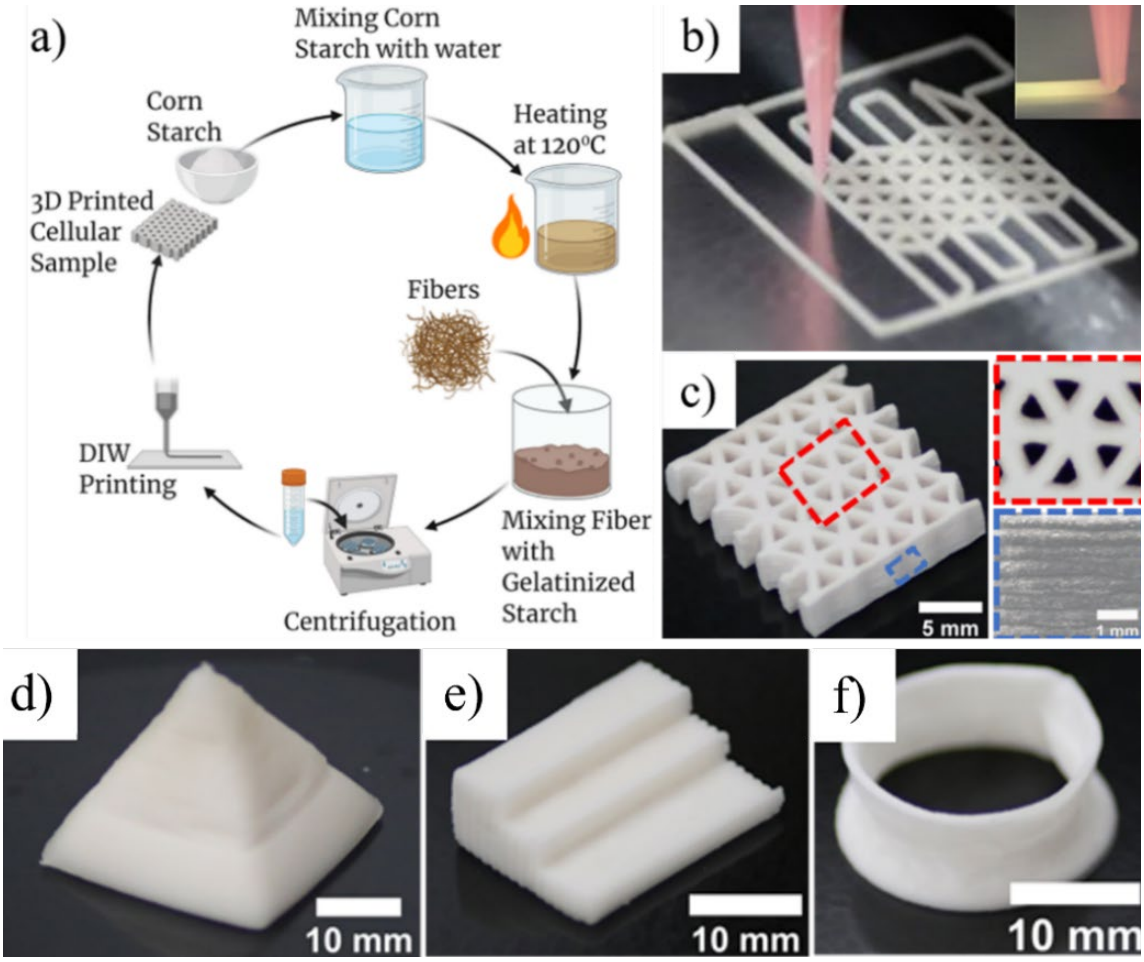

Figure 3.3: (a) A flow chart of the 3D printable inks formulated using entirely sustainable resources (corn starch, corn husks extracted cellulose fibers, and water) via a heat treatment process. (b) 3D printing of bio composites. (c) Optical images of a 3D printed cellular structure. The top view reveals the unit cell of the cellular structure, while the side view illustrates filament formation from bottom to top.

3.3.2 *Ink formulation, rheology and printability:* With the cellulose fibers extracted from corn husks, we proceeded to formulate 3D printable inks through a process outlined in 3-3a. Figure 3-1c and Figure 3-3b illustrate the 3D printing process of the composite ink, composed of corn starch with 10wt% cellulose fibers (CS-CF10), into a triangular cellular structure. The inset in Figure 3-3b clearly shows formation of the filament that retains its shape after extrusion from the nozzle.

The resultant inks exhibit 3D printability and are able to fabricate multilayered cellular structures (Figure 3-3d-f). The rheological properties of these inks play a pivotal role in formulating 3D printable inks for DIW. This AM method uses viscoelastic ink to fabricate 3D object in a layer by layer deposition manner[11,19,26]. Due to induced shear stress at the nozzle, the ink can be extruded from the nozzle at ambient conditions and turn into a gel-like material to retains its shape after extrusion[11,19,26].

The printable materials need to have shear thinning and yielding properties within a reasonable range of yield strength. Achieving suitable printability for direct ink writing (DIW) necessitates the attainment of specific ink rheology to prevent clogging during printing and to maintain the integrity of printed shapes post-extrusion. To optimize the rheological properties, we utilized the gelatinization phenomenon of amylopectin, which involves a chemical chain relaxation process induced by thermal and mechanical effect[11,35,74,75]. Corn starch is a heterogeneous material that consists of both linear (amylose) and highly branched (amylopectin) structures[74,75,90] (Figure 3-1b). When amylopectin in corn starch is heated with water, its dual helical crystalline structured side chains open and become a gel like viscoelastic material. Amylopectin undergoes retrogradation upon cooling, and its branches revert to their original dual helical structure[74,75](Figure 3-1b). Moreover, thermal processing of corn starch is essential to tuning the 3D printability and mechanical properties of the printed materials. The gelatinized amylopectin molecule interacts with cellulose fibers and other amylopectin molecules via hydrogen bonds, leading to different rheology and tunable mechanical properties of the materials[11,75]. Therefore, we tuned the ink rheology with water and preheating conditions for composites with different fiber fractions (Table 1 and 2).

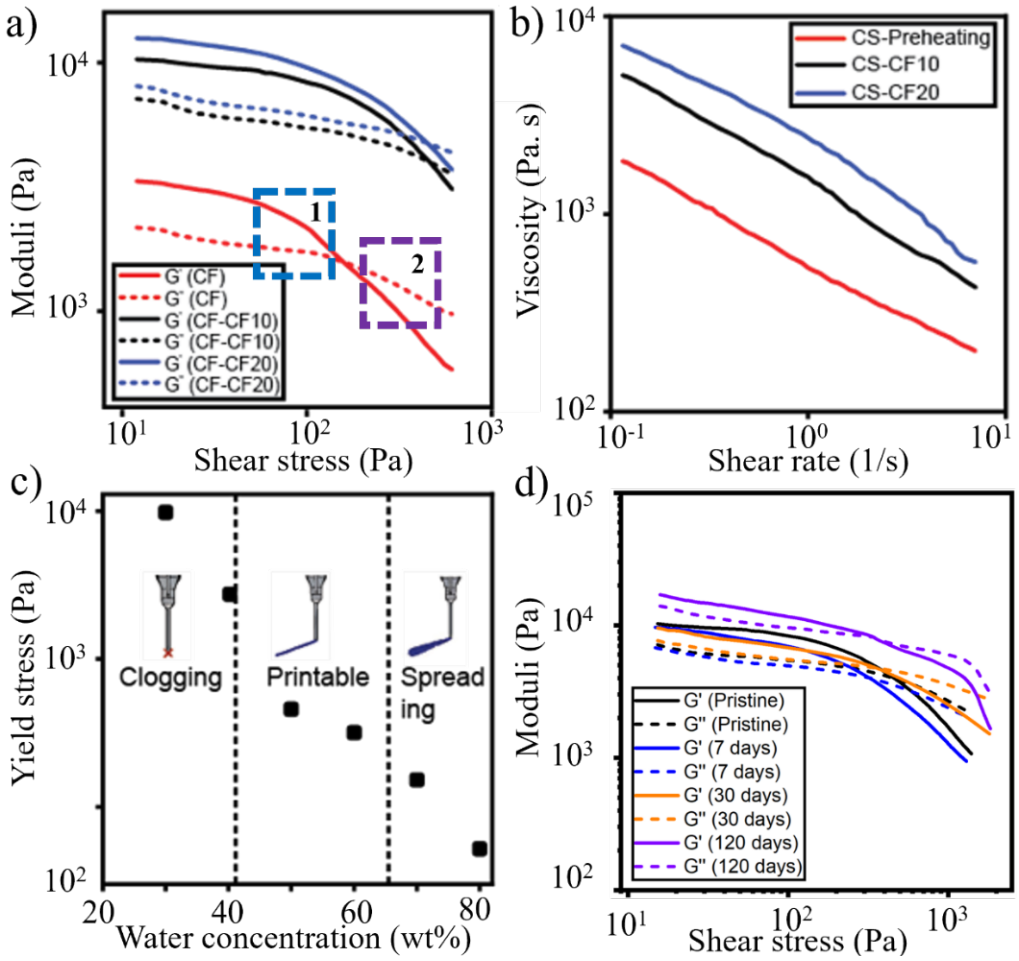

Figure 3.4: Rheological measurements of the inks show the (a) shear yielding behavior and (b) shear thinning properties. (c) 3D printability mapping showing water concentration and critical yield stress for printable inks. d) Aging effect on ink rheology and 3D printability.

Rheological analysis of the inks indicates a transition from a gel-like to a fluid-like state under shear stress. Figure 3-4a compares the storage modulus (G') and loss modulus (G") of pure corn starch (CS), CS-CF10, and CS-CF20 inks in relation to shear stress. The gel-like behavior of the inks is apparent when the storage modulus surpasses the loss modulus. Upon exceeding the yield stress, both moduli decrease significantly, with the loss modulus becoming dominant, indicating a transition to fluid-like behavior during extrusion. Additionally, the inks exhibit shear-thinning behavior, with viscosity decreasing notably at higher shear rates, ensuring smooth ink

flow (Figure 3-4b). To quantitatively evaluate printability, Figure 3-4c illustrates 3D printability mapping for CS-CF10 as a function of shear-yielding properties and various water concentrations. A low water concentration results in high shear-yielding stresses (>2745 Pa) due to the formation of large aggregates by CF fillers, leading to nozzle clogging and printing failures (Figure 3-3.5c). Conversely, a higher water concentration leads to a lower shear-yielding stress (<318 Pa), resulting in filament spreading post-extrusion and the failure of 3D structures (Figure 3-4c). Therefore, we determined that an intermediate water concentration (40-65wt%) for CS-CF10 provided favorable rheological properties and ensured 3D printability.

3.3.3 *Ink aging effects on rheology and 3D printability:* Corn-based 3D printable inks are of significant interest due to their extended shelf life. These materials can be stored at -20°C for more than two months without compromising their 3D printability. In our study, we investigated the effect of ink aging on both rheology and 3D printability, observing how these properties change over time. Rheological analysis conducted over a period of 120 days indicates that the inks maintain excellent printability comparable to pristine ink (Figure 3-4d). Like the pristine ink, rheological measurements of the stored inks reveal a transition from gel-like to fluid-like behavior under shear stress. Figure 3-3.6d provides a comprehensive comparison, focusing on the storage modulus (G') and loss modulus (G") of the inks stored for 7, 30, and 120 days with respect to shear stress. In all instances, the stored inks exhibit a gel-like response, where the storage modulus exceeds the loss modulus. Upon surpassing the yield stress, both moduli undergo a significant decrease, with the loss modulus predominating over the storage modulus. This transition indicates the shift towards fluid-like behavior during extrusion. Crucially, all stored inks retain favorable 3D printability when utilized in Direct Ink Writing (DIW). These results support the promising stability of the inks over an extended period, making them suitable for practical applications in 3D

printing.

3.4 Chapter Conclusion: In summary, we have developed sustainable and 3D printable composites solely from corn starch and cellulose fibers derived from corn husks. By leveraging the unique gelatinization process in the amylopectin molecules and thermally activated interactions between amylopectin and cellulose fibers, we achieved the desired ink rheology for 3D printing in DIW. Rheological analysis revealed that the formulated inks exhibited shear thinning and yielding properties essential for direct ink writing (DIW), ensuring smooth ink flow during extrusion and the retention of printed shapes post-extrusion. Our investigation on the ink aging effect demonstrated excellent shelf stability of the corn-based inks over a prolonged period without compromising printability. Overall, the findings highlight the potential of utilizing agricultural waste-derived cellulose fibers in the development of sustainable and high-performance 3D printable materials.

Chapter 4: Thermo-Mechanical Effect on Mechanical Characterization

4.1 Chapter Introduction: This chapter describes the process-property-microstructure relationship of the 3D printed corn-based composites. Our exploration commences with an examination of how the choice of filler affects the mechanical properties of the starch matrix. Subsequently, we analyze the influence of filler fraction on the overall properties of the composite materials. To evaluate the bending properties of the composites, we compare the results with both the rule of mixing and the Halpin-Tsai model. Additionally, we assess the stiffness (E), strength (σ), and toughness of cellular structures, drawing comparisons with classical cellular mechanics scaling laws. Following these investigations, we introduce a novel method for thermally strengthening 3D printed corn-based composites through a process that integrates thermal treatment with Direct Ink Writing (DIW) printing. This innovative approach allows for precise control over the microstructure of composites, thereby enhancing their mechanical robustness. The technique capitalizes on the thermal treatment's influence on hydrogen bonding interactions, both between amylopectin molecules and at the amylopectin-cellulose interfaces. The results of this study reveal the potential to achieve a tunable microporosity increase of over twofold, along with a substantial improvement in mechanical properties by more than threefold. This simple yet effective method holds the promise of developing environmentally friendly-mechanically robust materials for additive manufacturing.

4.2 Materials and Methods:

4.2.1 Printable ink formulation, rheological properties characterization and 3D printing details are in section 3.2.4 to 3.3.7.

4.2.2 *Solidification:* Biocomposites are sensitive to moisture removing rate. Drying corn-based composite at room temperature may cause dimensional changes and damages, including micro

cracks, bending, and twisting[11,84–88]. In order to control dimensional stability, we used a multistep freeze-drying process and removed moisture at a controlled rate using a freeze dryer (Harvest Right®, HRFD-Med-SCI). The samples were first frozen at -40ºC for 10 hours in vacuum followed by three steps drying process at -34ºC for 16 hours, 25ºC for 2 hours and 48ºC for 2 hours. After freeze drying, 10 min preheated specimens showed a uniform linear shrinkage of 5.6 ±1.9%. Then, samples were dried again at over 100ºC for 1 hour for complete removal of moisture.

4.2.3 *Mechanical properties characterization:* We performed the uniaxial compression and 3-point bending tests on the 3D printed samples. The sample surfaces were smoothed with sandpaper before compression testing to achieve an even and uniform contact between the sample surfaces and the compression plates. Compression tests were performed with the stroke rate of 1 mm/min in a universal testing machine (Shimadzu®). For triangular cellular samples, stress and strain were calculated from force-displacement curves, normalizing by the sample's cross section area and height. The bending specimens were prepared as per ASTM D7264/D7264M–21 and tested with the stroke rate of 1 mm/min. Flexural properties (stiffness and strength) were calculated from force-displacement curves using equations described in ASTM D7264/D7264M–21. The dimensions of our specimens are 20 mm x 16 mm x 4 mm for compressive cellular samples and 50 mm x 5 mm x 1.56 mm for flexural samples. At least three samples from each type of composites were measured in compression and in bending tests.

4.2.4 *Microstructure characterization:* The structures of the extracted cellulose fibers and 3D printed corn-based composites were taken by a scanning electron microscope (FEI Quanta 200 ESEM). Prior to the imaging, both the fibers and the composite surfaces were coated with ~5 nm carbon sputtering in an ion sputter (Gatan 682 Precision Etching Coating) to avoid charging in SEM. Fiber dimensions and composite pore sizes were measured using ImageJ software.

4.2.5 *Hydrogen bonding characterization:* Cellulose fibers, 6 to 14 minutes preheated composites were grounded by mortar before subjected to the Fourier-transform infrared spectroscopy (FTIR) analysis. Afterward, they were heated in an oven (Huanghua Faithful Instrument Co., LTD) at 100°C for 30 minutes to remove moisture and grounded again to make finer powder. FTIR was performed using a Thermo Nicolet 6700 to characterize the removal of lignin and hemicellulose from corn husk fibers and the hydrogen bonding functional groups in the composites.

4.3 Result and Discussion:

4.3.1 *Compressive properties:* We printed triangular cellular structures for compression tests with a range of fiber fractions and relative densities to quantify the scalability of the composites. Representative stress-strain curve of CS-CF10 samples is shown in Figure 4-1a that is measured under compression loading. Figure 4-1b shows the results for specific strength and stiffness for the biocomposites along with the control samples produced using the pure corn starch. Both 10wt% RF- and CF-reinforced composites exhibit a significant increase in specific stiffness over the control samples from 210±15 to 538±35 and 648±123 MPa·cm^3/g, respectively (Figure 4-1b). Similarly, the specific strength enhances by 56% and by 119.3% in RF and CF composites, respectively (Figure 4-1b). Compared with RF, CF shows a significant improvement in mechanical reinforcement effect. We attributed this to two aspects that i) the chemical treatments removing hemicellulose and lignin, which resulted in mechanically strong cellulose fibers, and ii) the formation of hybrid micro-nanofibers and rough surfaces in CF, which led to more reactive sites on surfaces and stronger mechanical interlocking and adhesion with the matrix[36]. Furthermore, we fabricated triangular cellular structures with varying fiber fractions. Compression test results indicated that cellular composites with 20wt% cellulose fibers exhibited 3.3- and 4.4-times

enhancement in specific strength and stiffness, respectively, over the printed pure matrix material (Figure 4-1c).

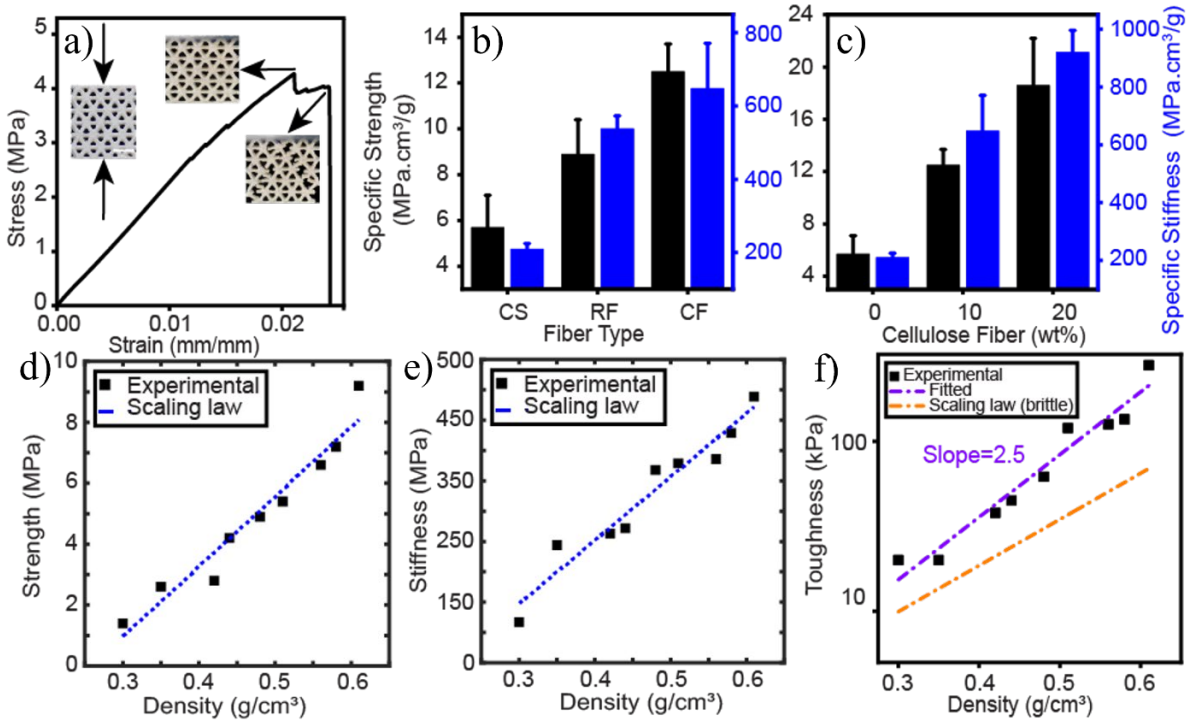

Figure 4.1: (a) A representative stress-strain curve of CS-CF10 triangular cellular structure with screenshots of cracks propagation during compression. (b) Measurement of specific strength and stiffness for 3D printed pure corn starch (CS), RF and CF reinforced composites (10 wt% fibers), and (c) CS-CF composites at different fiber fractions. Measurements of (d) strength, (e) stiffness and (f) toughness of 3D printed cellular structures with different densities.

Interestingly, the cellular structures showed a progressive failure pattern as shown in a representative stress-strain curve for CS-CF10 in Figures 4-1a and 4-2a-b, in contrast to brittle materials that fail immediately at the maximum strength. We observed multiple cracks initiation sites throughout the samples and the major crack propagated progressively along a deflected path or derived into multiple cracks (Figure 4-2a-b). We also print cellular materials with different relative densities for the purposes of lightweight material and scalability tests. The strength,

stiffness and toughness all increase with increasing nominal densities (Figure 4-1d-f). The strength and stiffness of the triangular cellular structures follow the classical cellular mechanics scaling law[11,26,94] (equation 7-8). Due to the progressive crack propagation before failure, higher toughness is measured compared to the scaling law for brittle materials (Figure 4-1f, Figure 4-2a-b). The enhancement in toughness is more significant for the samples with higher density.

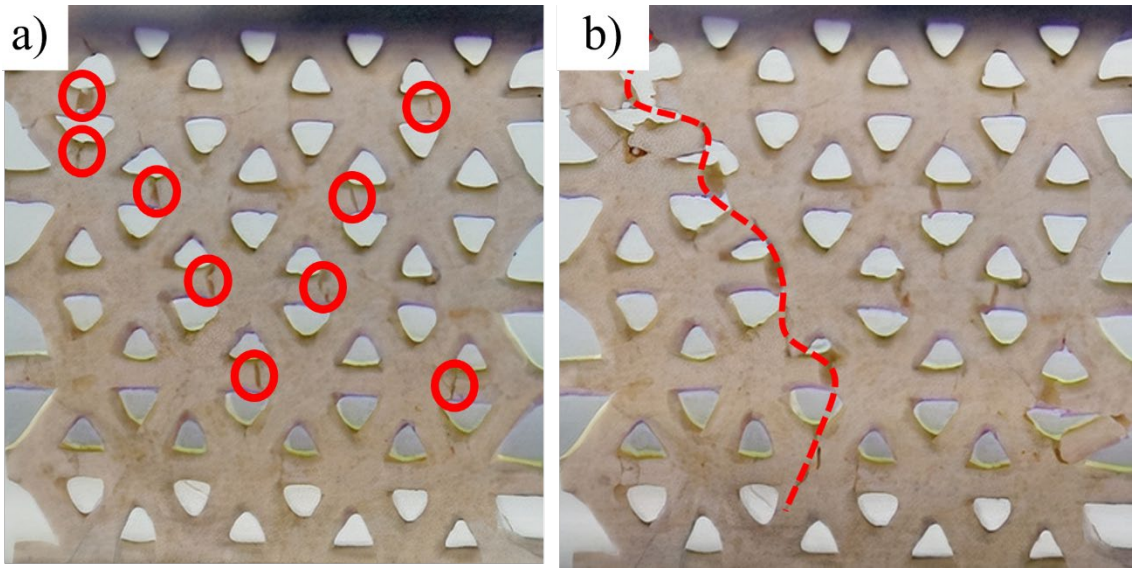

Figure 4.2: Fracture behavior of 3D-printed triangular cellular composites. a) Multiple cracks initiation sites and b) crack propagation along a deflected path.

Scaling law of cellular structures:

The scaling law of strength and stiffness of the triangular cellular structures are:

$$E = \mathrm{B}\left(\frac{\rho}{\rho_s}\right)^b E_s \qquad \text{(Eq. 7)}$$

$$\sigma = \mathrm{C}\left(\frac{\rho}{\rho_s}\right)^c \sigma_s \qquad \text{(Eq. 8)}$$

where E_s, σ_s and $\rho_s$are the stiffness, strength, and density of the bulk solid material, respectively. For triangular structures, b =1 and c =1.[26] For perfectly linear elastic brittle materials, the toughness is

$$T = \frac{\sigma^2}{2E} \qquad \text{(Eq. 9)}$$

4.3.2 *Flexural properties:* We manufactured rectangular solid beams for bending tests to evaluate flexural properties. Similar to compression samples, the strength and stiffness of bending specimens exhibited an increase with increasing fiber fraction. In bending tests, we observed monolithic enhancement up to 4.2 and 2.8 times increment in flexural strength and stiffness, respectively for 20wt% of cellulose fiber reinforced composite (Figure 4-3a). To validate our experimental results, we compared them with the predictions of the rule of mixture (ROM) and Halpin-Tsai's model. Remarkably, the experimental results fell within the theoretical range predicted by both the ROM and Halpin- Tsai's model[91,92] (Figure 4-3b-c).

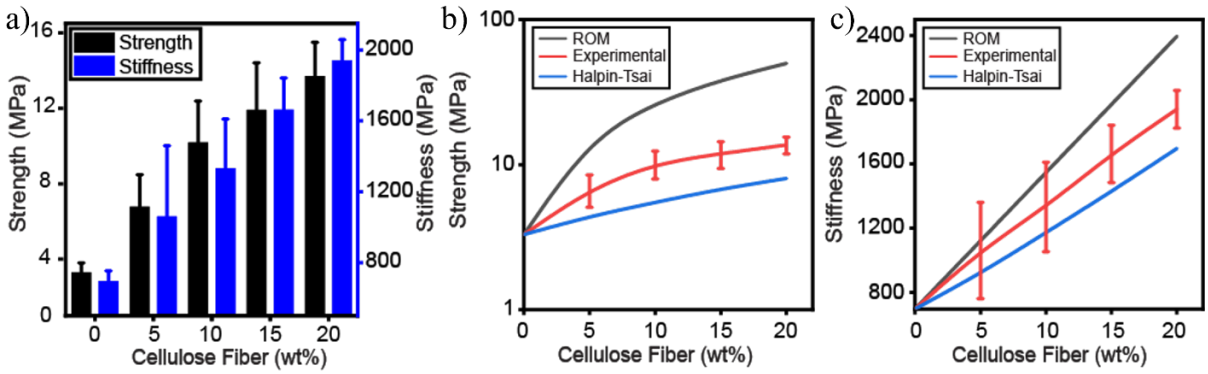

Figure 4.3: (a) Measurement of the flexural strength and stiffness at different fiber fractions. Comparison of experimental measurements of (a) flexural strength and (b) stiffness with the theoretical bounds.

Rule of mixture (ROM):

$$E = E_f V_f + E_m V_m \quad \text{(Eq. 1)}$$

$$\sigma = \sigma_f V_f + \sigma_m (1 - V_f) \quad \text{(Eq. 2)}$$

Halpin-Tsai's model:

$$\frac{E}{E_m} = (1 + \eta\zeta V_f) + (1 - \eta V_f) \quad \text{(Eq. 3)}$$

$$\frac{\sigma}{\sigma_m} = (1 + \eta\zeta V_f) + (1 - \eta V_f) \quad \text{(Eq. 4)}$$

where,

$$\zeta = 2\left(\frac{l}{d}\right) \quad \text{(Eq. 5)}$$

$$\eta = \left(\frac{E_f}{E_m} - 1\right) / \left(\frac{E_f}{E_m} + \zeta\right) \quad \text{(Eq. 6)}$$

and E, E_f, E_m, σ, σ_f, and σ_m are stiffness and strength of composite, fibers, and matrix, respectively. The parameters l and d represent the fiber length and diameter, and V_f and V_m are volume fractions of fibers and matrix in the composite. For cellulose fibers, 9.2 GPa and 237.4 MPa were used as the stiffness and strength[93]. We experimentally measured strength and stiffness for amylopectin and cellulose fibers dimensions in the Halpin-Tsai's model.

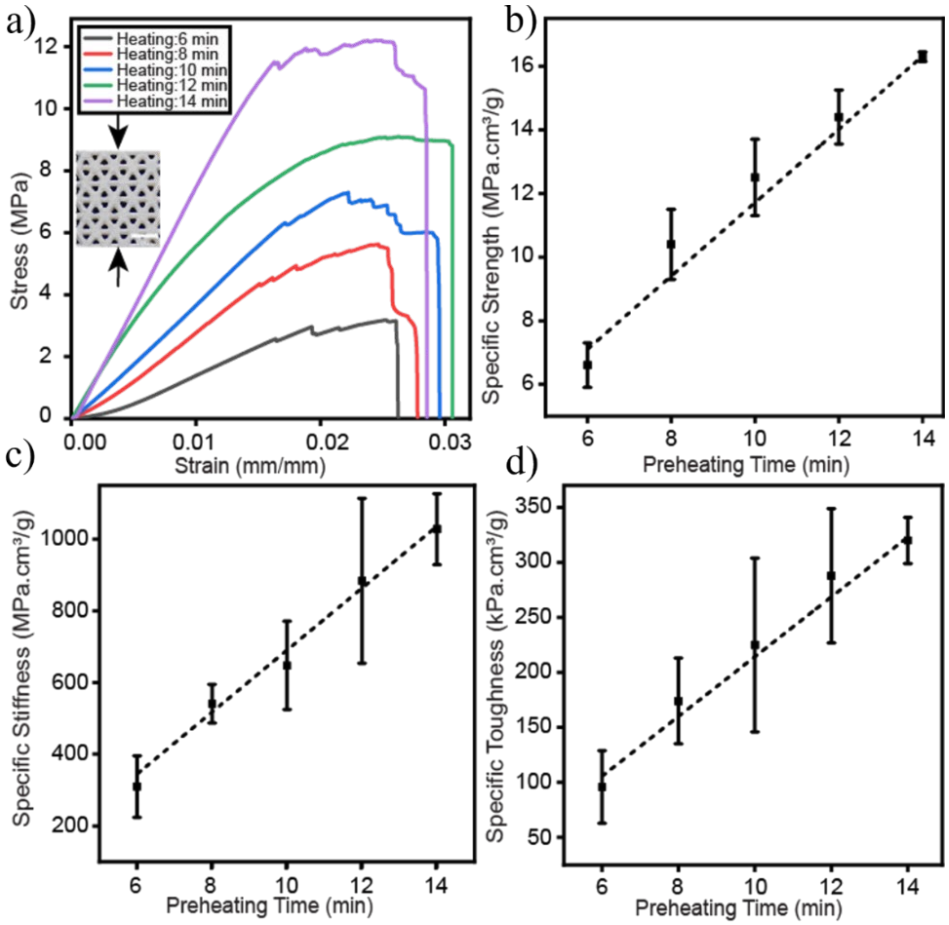

Figure 4.4: (a) Stress strain curves for CS-CF10 composites formulated at different preheating conditions and the measurements of (b) specific strength, (c) specific stiffness, and (d) specific

toughness. The results show a wide range of mechanical tunability via a thermal process during ink preparation.

4.3.3 *Thermal tuning composite properties:* We investigated the thermal treatment effect on tuning mechanical properties. Representative stress-strain curves of CS-CF10 samples with preheating time 6-14 min are shown in Figure 4-4a. Despite their identical compositions, a longer preheating treatment leads to a more pronounced progressive failure pattern and substantial increases in the mechanical properties. The specific strength, stiffness, and toughness increase linearly as the preheating time (Figure 4-4b-d). Such simple but effective thermal treatment resulted in tunable ranges of 2.5, 3.3 and 3.3-fold in specific strength, stiffness, and toughness, respectively. We attribute this tunability to the porous microstructures and hydrogen bonds formed at the amylopectin molecule-molecule and cellulose-amylopectin interfaces as a result of the thermal treatment (Figure 4-5). The micropores of the samples are shown in the SEM images in Figure 4-5a-c. Our results showed that as preheating time increases, pore numbers and averaged pore sizes decreased, while composite density increased (Figure 4-5d). Via the simple preheating treatment during ink preparation, we achieved significant microstructure and density tunability ranges up to 2 folds in the printed specimens. In addition to microstructure and density tunability, preheating treatment greatly affects the fraction of hydrogen bonds formation at the fiber-matrix interface. The hydrogen bonds are responsible for strengthening the intra-matrix (i.e. between amylopectin molecules) and fiber-matrix interfaces[36,83,95,96] (Figure 4-5f). Such strengthening mechanism contributes significantly to the composite's mechanical properties[83,95,96]. Hydrogen bonding form when hydroxyl (OH) and carboxylic acid (COOH) groups are present in fibers and matrix[36,95,96]. Figure 4-5e shows FTIR spectrums for 6 to 14 minutes preheated samples. The O–H stretch for hydroxyl group appears as a band in the region 3000-3600 cm^{-1}, centered at

about 3299 cm^{-1}. Unlike the O–H stretch observed in the hydroxyl group, carboxylic acid O–H stretch is reflected a sharp peak at 2968-2881 cm^{-1}. FTIR analysis shows a monolithic increase of hydrogen bonding groups as an increasing thermal treatment time and thus strengthen the 3D printed composites. This thermally tunable behavior of the corn-based composites paves the way forward to design and develop sustainable composite materials with tunable mechanical properties.

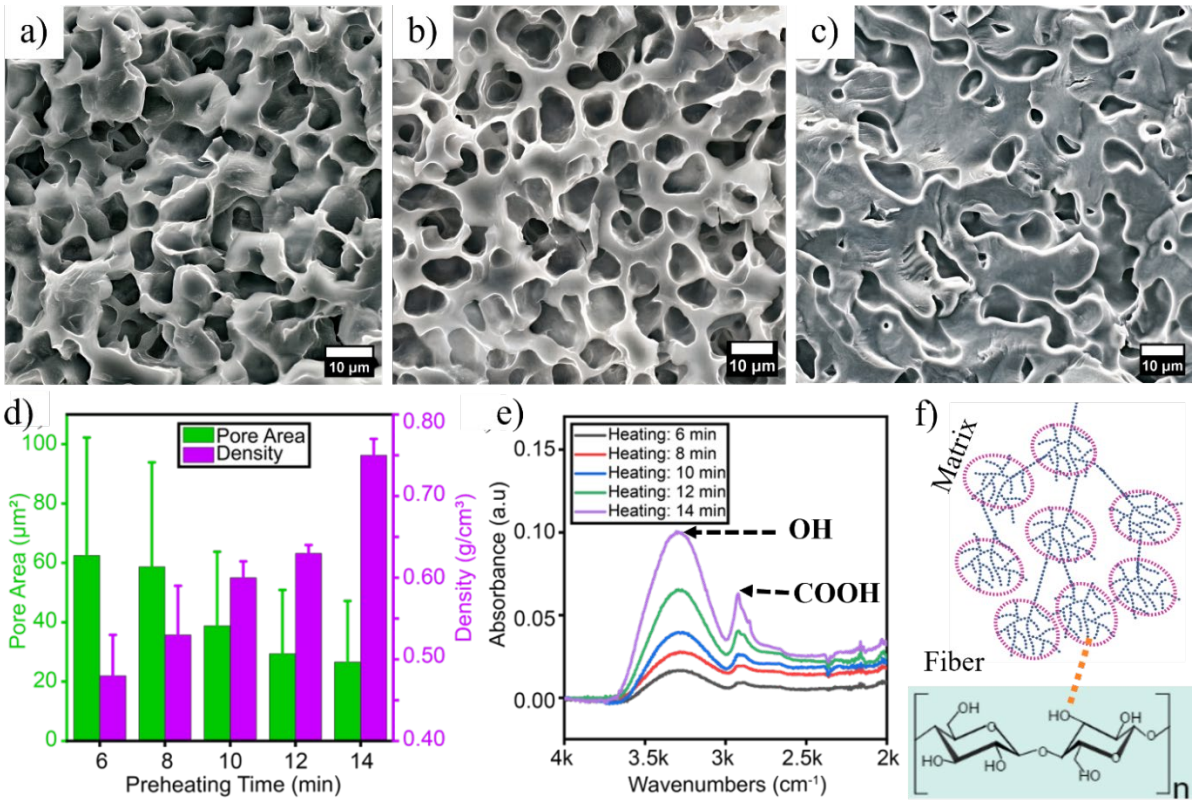

Figure 4.5: SEM images of 3D printed samples with (a) 6 min, (b) 10 min and (c) 14 min preheating. (d) Miro pore sizes and composite densities as a function of preheating time. (e) FTIR spectra showing increasing hydroxyl and carboxylic acid groups in samples with increasing preheating time between 6 to 14 min.(f) Schematic of hydrogen bonds formation at fiber matrix interface.

4.3.4 *Aging effect on composite mechanical properties:* We preserved formulated ink for an extended period (up to 120 days) at -20°C to assess the effect of ink aging on both their 3D

printability and mechanical properties. The ink aging effect on printability is briefly discussed in section 3. Subsequently, we conducted mechanical characterization of the 3D printed corn-based composite. Figure 4-6a illustrates stress-strain curves for both the pristine and aged composites. In Figure 4-6b, we compared the specific strength and stiffness results for both the aged composites and the pristine samples. Notably, the stiffness of the material remained relatively consistent, showing minimal variation throughout the aging period. However, we observed a slight degradation in the material's strength, with a maximum decrease of 20% in specific strength observed in the stored composites over time.

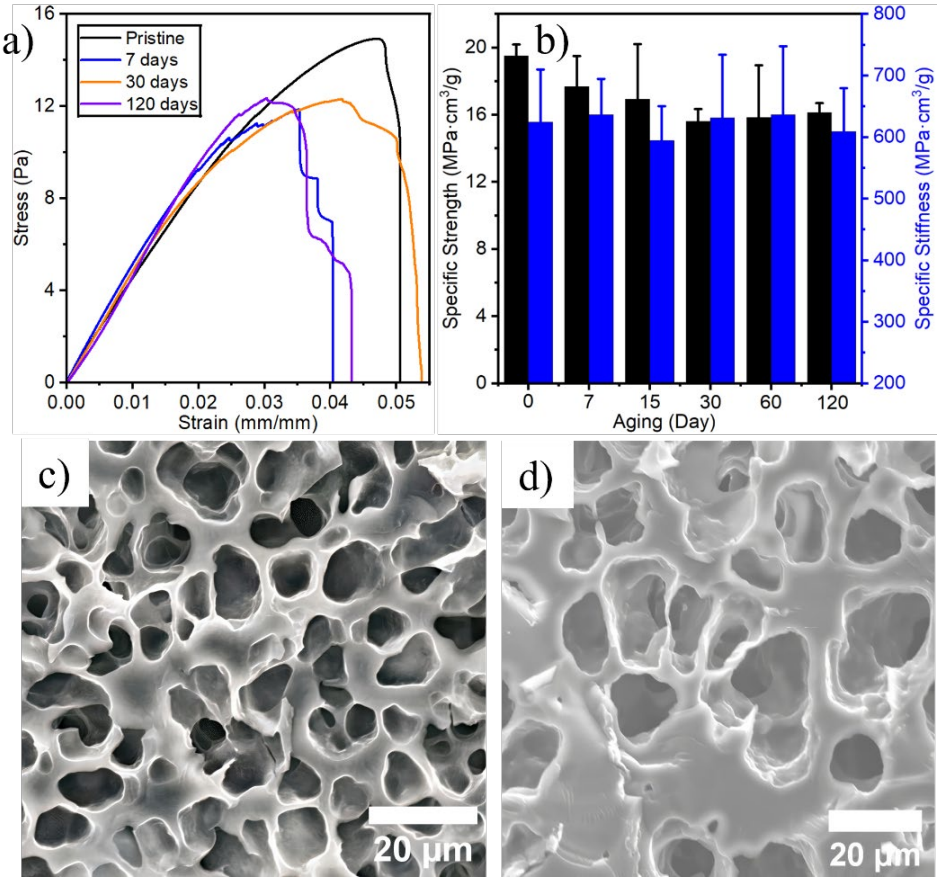

Figure 4.6: Aging effect of the composite mechanical properties. (a) Stress-strain curves of both the pristine and aged specimens are presented, along with (b) measurements of specific strength

and specific stiffness. SEM images illustrating the microstructure of (c) pristine and aged specimens after (d) 30 days. All composite contains 10%wt of cellulose fibers.

Specifically, the specific strength displayed a continuous decreasing trend when compared to the pristine samples, decreasing from 19.5 ± 0.7 MPa cm^3/g to 16.2 ± 1 MPa cm^3/g, as recorded at 7 and 120 days, respectively. This decline in specific strength can be attributed to the porous nature of the composite microstructure, underscoring the importance of comprehending the process-property-microstructure relationship. To further investigate this relationship, we performed microstructure characterization. SEM analysis (Figure 4-6c-d) revealed the porous nature of the composite materials. However, the micropores of the samples exhibited differences in pore size compared to the pristine ones, despite undergoing identical thermal treatment. We attribute these observed changes in the mechanical properties of the corn-based composites to the nonuniform activation of the amylopectin molecules in the aged specimens. This occurred during the uncontrolled unfreezing step at room conditions before conducting the thermal treatment in the oven at 100°C for 10 minutes of preheating.

4.4 Chapter Conclusion: In summary, we have developed 3D printable composites reinforced with raw fiber (RF) and cellulose fibers (CF). The experimental findings revealed a notable increase in specific stiffness for both RF and CF-reinforced composites compared to the control samples. However, CF exhibited a significantly enhanced mechanical reinforcement effect compared to RF. We attribute this improvement to the higher proportion of mechanically robust cellulose fibers in CF, as well as the formation of hybrid micro-nanofibers and rough surfaces, which provided more reactive sites for stronger mechanical interlocking and adhesion with the matrix. By leveraging the unique gelatinization process in the amylopectin molecules and thermally activated interactions between amylopectin and cellulose fibers, we achieved tunable

material properties in substantial ranges for the printed composites. We observed these interactions significantly depend on the thermal treatment conditions. The process-structure-property relationships showed that by using a preheating process the microstructures could result in micropore sizes of 26.6−62.5 μm^2 and material densities of 0.48−0.75 g/cm3. SEM images exhibited distinct microstructural changes, and FTIR measurements clarified hydrogen bond formations under various preheating conditions. Therefore, the mechanical properties were tunable in ranges of 2.5−3.3 folds in specific strength, stiffness, and toughness. Furthermore, the experimental compressive properties of cellular samples were found to be tunable based on the relative density of the cellular sample. Those compressive properties (strength and stiffness) follow the classical cellular mechanics laws. Moreover, flexural properties measurements demonstrated a remarkable increase, with the 3D printed 20wt% cellulose fiber composites exhibiting over a 4.2-fold increment in flexural strength and a 2.8-fold increment in flexural stiffness compared to the control sample.

Chapter 5: Tunable Porous 3D Structures with Multiscale Porosity

5.1 Chapter Introduction: Porous biomaterials have emerged as versatile platforms with vast potential across diverse fields, spanning from biomedical applications to energy-related technologies due to their distinctive porosity-driven functional properties. Tailorable pore sizes and distributions are critical features in designing functional and biocompatible tissue scaffolds, drug delivery systems, and microfluidic devices[29,37,38,60-66]. For instance, porous scaffolds play a vital role in bone regeneration applications by facilitating processes like oxygen and nutrient exchange, cell migration, and waste product expulsion, where pore sizes and interconnectivity dictate cell behavior and tissue formation[29,63-64]. In drug delivery systems, controlled release of therapeutic agents relies on voids within materials, with surface-to-volume ratios dictating drug release kinetics[37,63]. Microfluidic devices leverage capillary action mechanisms influenced by pore size and surface tension to manipulate fluid flow for various analytical and diagnostic applications[67]. Beyond biomedical domains, porous biomaterials find significant utility in energy-related fields, including sensors, supercapacitors, and batteries[62,72,73]. For example, hierarchical porous carbon materials derived from natural sources like starch offer exceptional specific surface areas and controllable porosities, enhancing energy storage and power density in supercapacitors[73].

Conventional options primarily rely on petroleum-derived polymers, posing challenges such as limited biodegradability, potential release of harmful byproducts, and biocompatibility issues, contributing to environmental pollution. In contrast, food-based materials offer a promising alternative due to their abundance, renewability, non-toxicity, biocompatibility, and biodegradability, effectively addressing concerns associated with petroleum-based counterparts. Precisely controlling porous structures is crucial for their effective use in advanced applications.

While kinetic and templating-based manufacturing methods have been prevalent for creating mesoporous materials, they face drawbacks like complexity, high costs, and chemical usage[71-72].

Recent advancements in amylopectin-based 3D printable bio composites have sparked interest in developing mechanically robust porous materials for additive manufacturing (AM), offering eco-friendly alternatives to current petroleum-based options[8,11,12,17,19,21-23,54-56]. AM, or 3D printing, enables precise structural designs, microstructural control, waste reduction, and rapid fabrication[44,45]. For instance, Khaled et al. demonstrated how 3D printing can revolutionize medicine manufacturing for personalized care by producing multi-compartment tablets with well-defined controlled drug release profiles[22,38].

This chapter describes how to achieve multiscale porosity in amylopectin-based composites through a thermally activated gelatinization process of amylopectin molecules coupled with 3D printing. By controlling printing paths, macropores are engineered, while degree of gelatinization governs micro and nanopores formation. Process-microstructure relationship reveals that longer preheating treatments at higher gelatinization temperatures significantly reduce micro pore area by over 2-fold and nanopore surface area by over 3-fold. The programmable porous corn starch-based composites hold immense potential across applications such as bone scaffolding, drug delivery, sensors, and batteries, marking a new era of functional biomaterial design and utilization.

5.2 Materials and Methods:

5.2.1 *Materials and Printable Ink Preparation:* The 3D printable composites were composed of amylopectin-rich corn starch and cellulose fibers derived from corn husk [24]. Initially, corn starch and water were mixed at specified ratios described in (Table 3) using a Flacktek® DAC 400.2 VAC mixer at 1800 rpm for 3 minutes. Subsequently, the ink underwent thermal treatment in a drying oven (Huanghua Faithful Instrument Co., LTD) according to the preheating conditions

outlined in Table 3. This preheating treatment induced gelatinization of amylopectin. Following heating, cellulose fibers were incorporated into the gelatinized corn starch. The resulting composite gels were then mixed at 2000 rpm for 2 minutes followed by 1500 rpm for 2 minutes using the mixer.

Table 3: Ink formulations with 10wt% of cellulose fibers at various preheating conditions.

Inks	**Amylopectin: Water**	**Temperature, (*^{o}C)***	**Time, (*min)***
1	1.5	80	10
2	1	100	10
3	0.8	120	6
4	0.8	120	10
5	0.8	120	12

5.2.2 *3D printing and Others:* Rheological properties characterization, 3D printing details, and solidification are in section 3.2.5, 3.3.6 and 4.2.2.

5.2.3 *Characterization of Microstructure:* The structures of both extracted cellulose fibers and 3D printed corn-based composites were examined using a scanning electron microscope (FEI Quanta 200 ESEM). Prior to imaging, the fibers and composite surfaces were coated with ~5 nm of carbon using an ion sputter (Gatan 682 Precision Etching Coating) to prevent charging in the SEM. Composite pore sizes were analyzed using ImageJ software.

5.2.4 *Porosity Characterization:* Surface area, pore volume, and nanopore size of the starch-based composites were determined using the Brunauer-Emmett-Teller (BET) and Barrett-Joyner-Halenda (BJH) method via N_2 adsorption onto the composites. The analysis was conducted using a 3Flex 3500 instrument (Micromeritics Instrument Corp., Norcross, GA) after degassing the composites at 150°C prior to N_2 adsorption.

5.3 Results and Discussion: The essential constituents for formulating these composites encompass amylopectin-rich waxy corn starch, cellulose fibers, and water (Figure 5-1a, Table 3). Upon subjecting amylopectin to heat in the presence of water, starch granules undergo gelatinization, a process that unfolds side branches, leading to the formation of an extensive network of gel balls. This exposes hydroxyl (-OH) and carboxylic acid (-COOH) functional groups, facilitating hydrogen bonding with amylopectin granules and cellulose fibers[11,21,74,75]. This interaction consequently converts the starch and water mixture into viscoelastic materials endowed with the desired rheological properties for 3D printing in DIW (Figure 3-1b), while also introducing a porous nature into the composite microstructure during the retrogradation process.

5.3.1 *Fabrication of 3D composite structure with multiscale porosity:* Utilizing the formulated inks, we have successfully produced cellular structures with multiscale porosity by using Direct ink writing (DIW) 3D printing method. In DIW, a viscoelastic material is extruded from a translating nozzle under shear stress at ambient room conditions, facilitating the fabrication of 3D designs through layer-by-layer deposition of material[11,21]. Figures 5-1a illustrate the 3D printing process of the corn-based bio composite into cellular structure. The inset in Figure 5-1a showcases an extruded filament from the nozzle that retains its shape. Figure 5-1b-e illustrates 3D cellular structures with diverse macroscale pores achieved through adjustments in print parameters like speed and ink extrusion, alongside printing path designs. For instance, Figures 5-1b-c showcase structures with distinct printing path designs but under identical printing conditions. Additionally, Figures 5-1c-d demonstrates structures with varying macropore sizes printed at different speeds (20 mm/s for Figure 5-1c and 10 mm/s for Figure 5-1d). This method enables precise control over macropore size, shape, and distribution within the resulting macroporous structure. Furthermore, the Scanning electron microscope (SEM) images in Figure 5-1f-g highlight the micro-scale pores

and cellulose fibers within the samples.

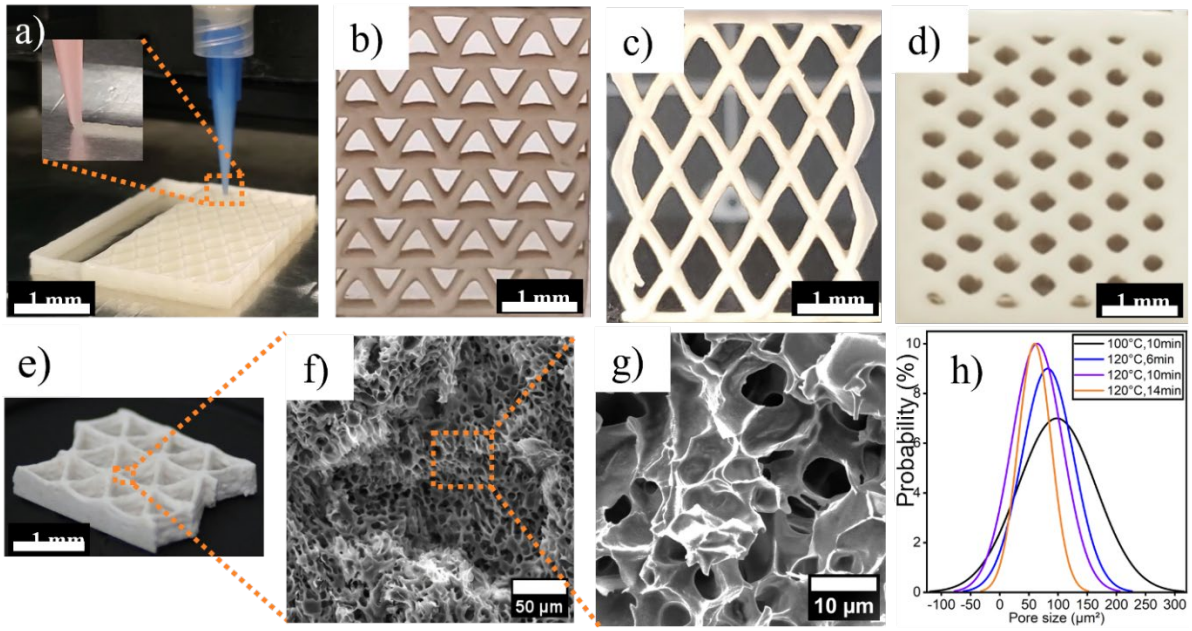

Figure 5.1: Fabrication of 3D composite structure with multiscale porosity a) 3D printing of corn-based composites. Multi-layer 3D structure: b-d) Macro scale pores in cellular structure via printing path design and printing parameter optimization. e) Optical images of a 3D printed cellular structure from top, and side views., and f-g) Cross-sectional SEM images display micro-scale pores and cellulose fibers within the samples. h) Normal distribution of micro-scale pore shows tailorable porosity based on gelatinization conditions during fabrication.

5.3.2 *Understanding amylopectin thermal activation mechanism on rheology:* The printability of ink in DIW relies on its shear-thinning and shear-yielding properties[11,21,26,28,47]. Rheological measurements, as depicted in Figure 5-2a-c, were conducted to evaluate the printability of the inks. Figure 5-2a-b demonstrates the transition of the starch-based materials from a gel-like to a fluid-like response under shear. Upon ejection from the printing head, the ink swiftly transforms from a fluid-like state to a solid-like material, maintaining its shape post-deposition-a phenomenon known as shear-yielding behavior.

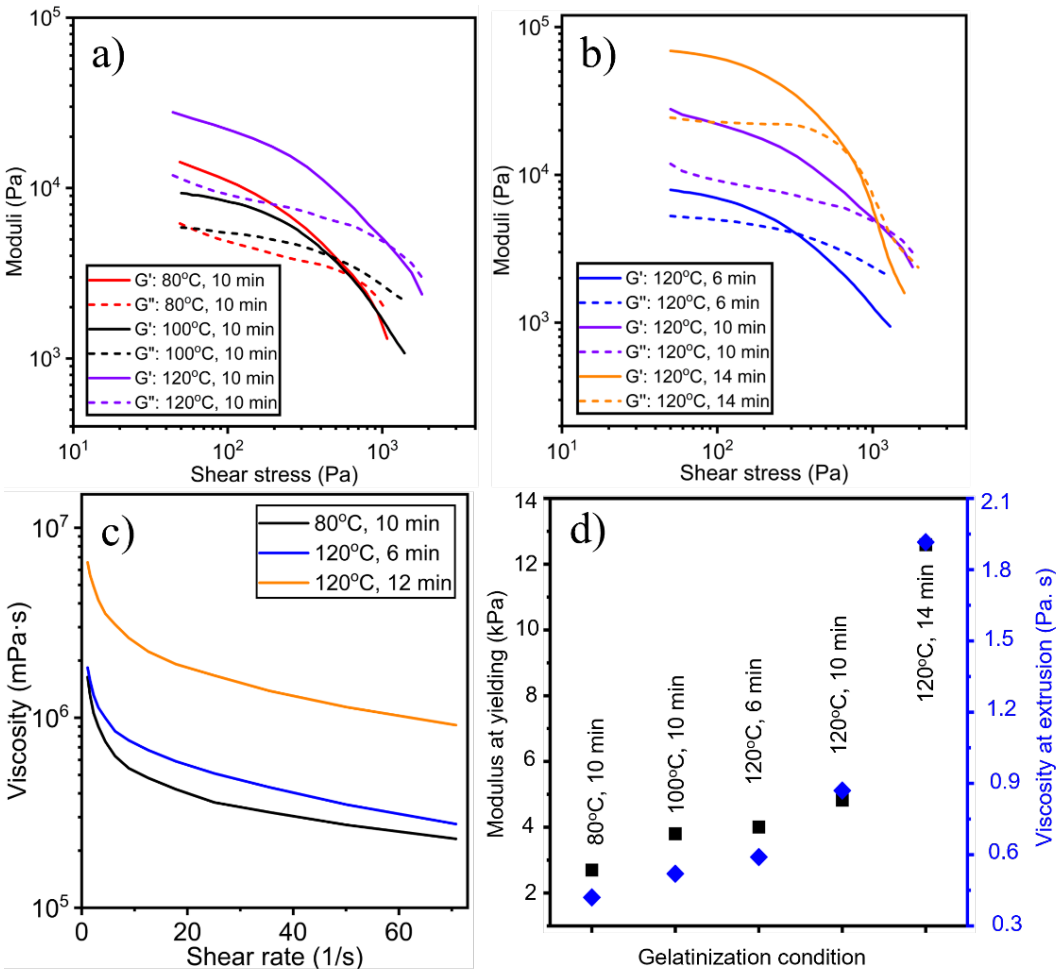

Figure 5.2: Rheological measurements of the inks showing (a-b) shear yielding (c) thinning behavior with gelatinization condition. (d) Ink properties (modulus and viscosity) at yielding changes with gelatinization condition.

Figure 5-2a-b illustrates the shear-yielding behavior of the composites, where the storage modulus (G') predominates over the loss modulus (G") before the crossover point of G' and G". Subsequently, both moduli exhibit a notable decrease. Beyond the crossover point, the loss modulus becomes dominant over the storage modulus, signaling the transition to a fluid-like behavior during extrusion. Figure 5-2c shows the shear-thinning behavior of the corn-based composites, wherein viscosity markedly decreases at higher shear rates. This characteristic facilitates smooth ink flow during the extrusion process. Rheological measurements in Figure 5-

2d indicated that the gelatinization parameters, notably temperature and duration, profoundly influenced inks' modulus and viscosity at yielding. For instance, despite identical composite compositions, increased and prolonged preheating treatments result in an exponential rise in both ink modulus at yielding and viscosity during extrusion (Figure 5-3d). These rheological shifts arise from the formation of hydrogen bonds among amylopectin molecules and fiber-matrix interfaces. The surfaces of amylopectin and cellulose fibers possess a notable concentration of hydroxyl (-OH) and carboxylic acid (-COOH) groups[11,21,74]. The extent of thermal influence during gelatinization significantly impacts the activation rate of hydroxyl and carboxylic acid groups formation[11,21,74]. Consequently, these groups engage in hydrogen bonding with amylopectin granules and cellulose fibers, thereby inducing varying degrees of rheological properties based on the level of gelatinization conditions.

5.3.3 *Understanding amylopectin thermal activation mechanism for micro to nano pores:* The degree of gelatinization plays a significant role in shaping the microstructure of the composite, akin to its impact on rheological properties. The degree of gelatinization is characterized by both gelatinization temperature and duration. In this section, we will briefly investigate each factor to achieve tunable multiscale porosity in composite structure.

5.3.3.1 *Gelatinization temperature effect on micro scale porosity:* We formulated 3D printable inks by preheating at 80, 100 and 120^{o}C for 10 minutes duration to investigate how gelatinization temperature affects the microscale porosity in the 3D printed composites (Table 3). Figure 5-3 demonstrates the influence of gelatinization temperature on the microstructure. Samples preheated to 80°C exhibit defects, well-defined grain boundaries, and lack porous characteristics (Figure 5-3a-c), attributed to the non-gelatinization behavior of amylopectin at temperatures below approximately 80°C[11,21,74]. As the preheating temperature increases, grain boundaries start to

merge, resulting in a porous microstructure. For instance, the SEM image of the sample preheated to 100°C shows partial grain boundary merging on the surface, alongside unregulated pore sizes and distribution in the cross-section (Figure 5-3d-f). Extending the preheating temperature to 120°C reduces voids on the surface, although partially merged granules are still observable. The microstructure remains porous in the cross-section as well (Figure 5-3g-i).

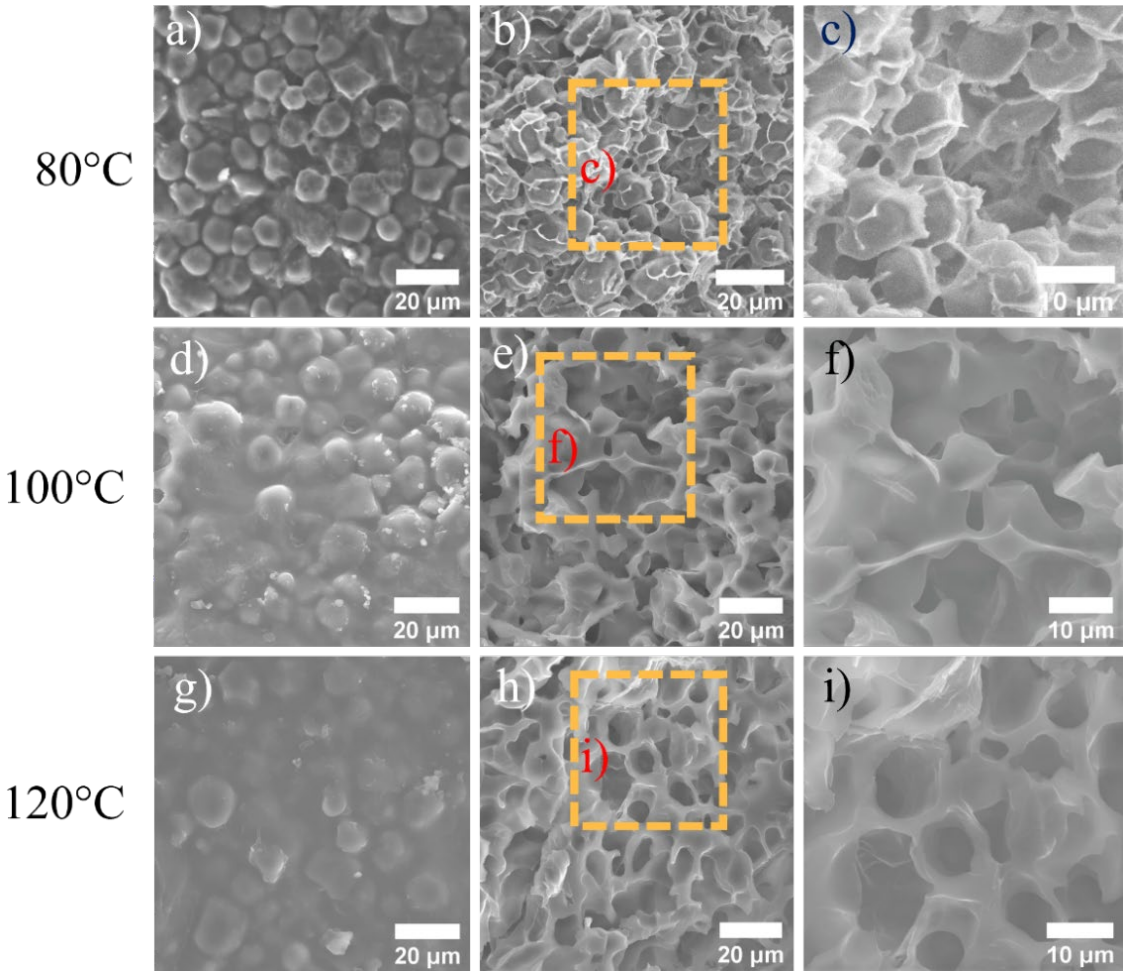

Figure 5.3: Investigating the effect of gelatinization temperature on retrogradation induced micropores into composite microstructure: Surface and cross-sectional SEM images of 3D printed samples, formulated at a-c) 80°C, d-f) 100°C and g-i) 120°C preheating for 10 minutes.

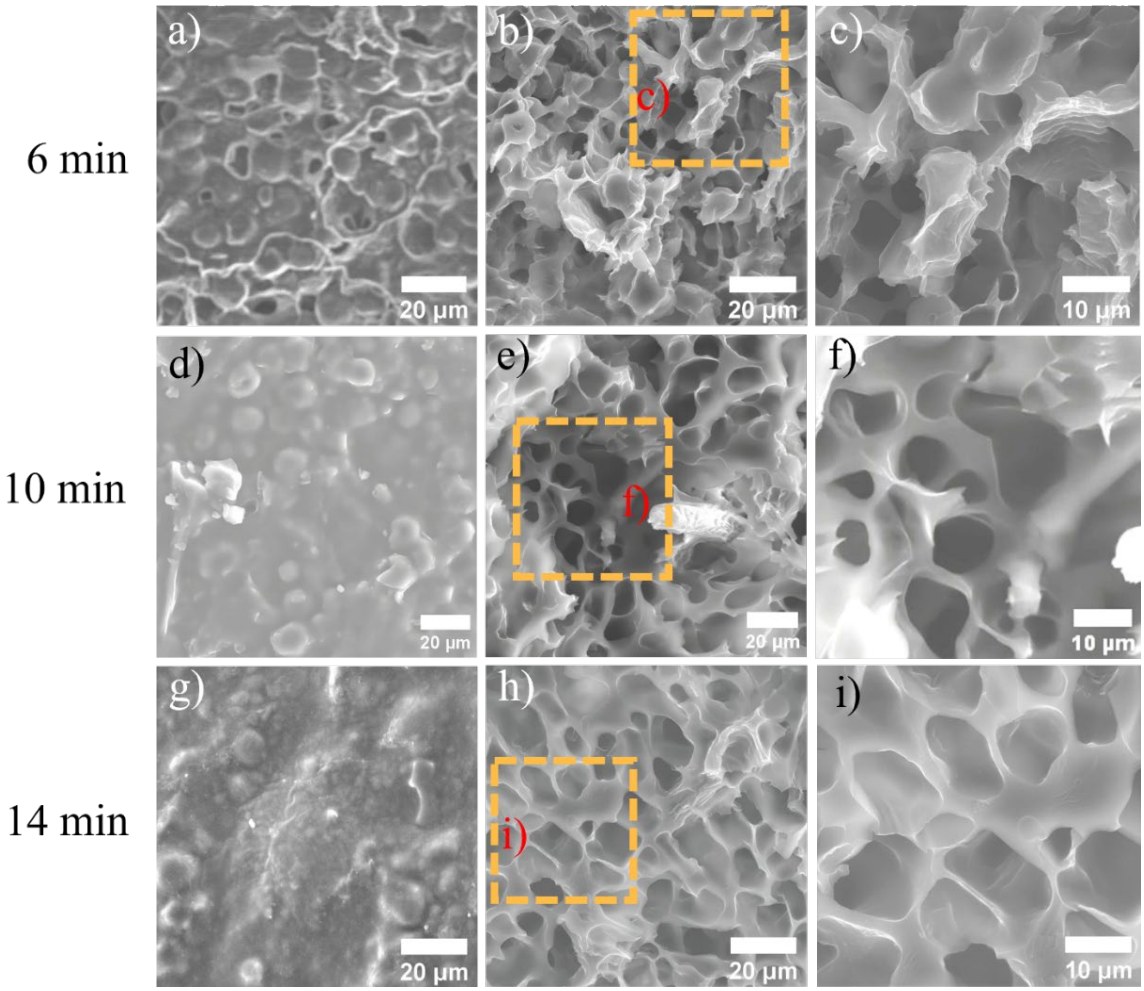

Figure 5.4: Investigating the effect of gelatinization duration on retrogradation induced micropores into composite microstructure: Surface and cross-sectional SEM images of 3D printed samples, formulated with a-c) 6 minutes, d-f) 10 minutes and g-i) 14 minutes of preheating at 120ºC.

5.3.3.2 *Gelatinization duration effect on micro scale porosity:* We examined the effect of preheating duration on tuning micropore size using an optimal gelatinization temperature of 120°C. Samples underwent preheating durations of 6, 10, and 14 minutes, revealing distinct microstructural changes through SEM analysis. Samples preheated for 6 minutes displayed numerous defects, partial grain boundaries between granules on the surface, and random-sized micropores in the cross-section. (Figure 5-4a-c). As preheating duration increased, there was a

noticeable change in micropore size. Extending the preheating time to 10 minutes resulted in partial merging of surface grain boundaries and a porous cross-section with more uniform micropore sizes (Figure 5-4d-f). Further extension to 12 minutes minimized voids, leading to fully merged grain boundaries and uniform micropores throughout the composite microstructure (Figure S1g-i). We conducted a comparative analysis of micropore sizes to understand the relationship between gelatinization conditions and microstructural characteristics. The comparative analysis of micropore sizes showed a significant trend: as preheating temperature increased from 80°C to 120°C for 10 minutes and preheating time increased from 6 to 14 minutes at 120°C, the average pore area decreased (Figure 5-1k). By adjusting gelatinization conditions during ink formulation, we achieved significant tunability over micropore sizes, with up to a 2-fold increase in printed specimen.

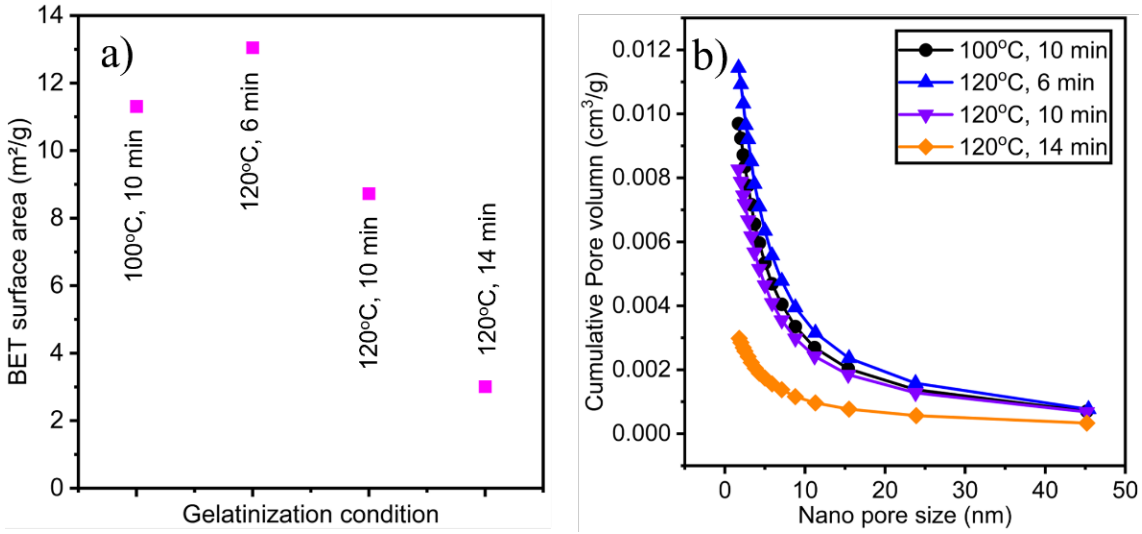

Figure 5.5: Investigating the effect of gelatinization conditions on retrogradation induced nanopores in composite microstructures: a) Surface area of nanopores and b) cumulative pore volume changes as gelatinization conditions intensified, measured using the Brunauer-Emmett-Teller (BET) and Barrett-Joyner-Halenda (BJH) method.

5.3.3.3 *Gelatinization conditions affect nano scale porosity: We* also explored the formation of

nanopores within the composite microstructure under varying gelatinization conditions. Similar to micropores, we observed a significant influence of gelatinization degree on nanopore formation during the retrogradation process. The analysis consistently revealed a decrease in the total BET surface area with increasing gelatinization temperature and duration (Figure 5-5a). For example, transitioning from a gelatinization condition of 80°C preheating for 10 minutes to a thermal treatment of 140°C for 14 minutes resulted in a decrease in the BET surface area from 11.4 to 3.0 m^2g^{-1} (Figure 5-5a). Furthermore, we observed a decrease in nanopore volume as the intensity of gelatinization conditions increased (Figure 5-5b). This trend is supported by the area under the curve of Figure 5-5b, indicating a steady decline in nanopore formation as the preheating temperature and time increase. However, the volume of nanopores is significantly dominated by the pore size of less than 10 nm indicating the formation large number of nanopore formation. This tunable porosity at micro and nanoscale within the microstructure was closely tied to the intensity of hydrogen bond formation among amylopectin molecules and cellulose fibers at the fiber-matrix interface, which could be modulated by controlling the activation rate of hydroxyl (-OH) and carboxylic acid (-COOH) groups through gelatinization conditions. This thermally tunable behavior exhibited by amylopectin-based composites holds significant promise for innovative solutions in the design and development of sustainable materials across various emerging applications.

5.4 Chapter conclusion: In summary, we introduced a process-microstructure guided manufacturing approach for manufacturing three-dimensional porous structures with hierarchical porosity, using food-based composite materials. By harnessing the thermally activated gelatinization process of amylopectin molecules coupled with 3D printing, we attained precise control over pore size at multiple length scales. This methodology enabled significant tunability

in macro, micro, and nano dimensions within the printed composites. The process-microstructure relationships showed that longer preheating treatments (14 minutes) at higher gelatinization temperatures (120°C) led to a notable reduction in micro pore area by over 2-fold and surface area of nanopores by over 3-fold. SEM images exhibited clear microstructural differences: Lower preheating temperatures (80°C) caused defects in composite microstructure, whereas higher temperatures (120°C) created porous structures with varying pore sizes. Longer preheating times (14 minutes) at high temperatures (120°C) reduced defects and introduced uniform micro and nanopores. The novel approaches reported in this study offer opportunities to achieve tailored porosity at macro, micro, and nano scales in composite microstructure. This underscores the potential for replacing petroleum-based polymers and represents a significant step towards sustainable manufacturing practices. With the rising demand for eco-friendly solutions, these food-based composite materials offer practical alternatives with diverse applications across advanced engineering and biomedical fields.

Chapter 6: Recycling 3D Printed Corn-Based Composite.

6.1 Chapter Introduction: Petroleum-derived plastics are being used extensively in our lives in numerous ways, despite their threats to the environment, marine biology, and human health[1–3]. The use of these plastics has skyrocketed since the 1950s, with a staggering 400 million metric tons produced in 2022 alone. However, their slow decomposition, spanning centuries, raises significant environmental concerns. Thus, materials recycling and resource efficiency has become a sustainable approach for petroleum-based plastic in order to reuse rather than relegated to the environment. However, petroleum-based composite recycling faces key challenges, such as the difficulty of separating fiber and matrix from their structures to allow for recycling after service life[4]. Despite efforts, the actual recycling rate remains low, with only a fraction of plastics (less than 9%) being recycled annually, leading to significant waste accumulation. Moreover, recycling petroleum-based plastics involves complex processes, heavy chemical usage, and high energy consumption, contributing to environmental pollution and escalating costs. Additionally, studies indicate that recycled petroleum-based materials often experience a degradation in mechanical properties over successive recycling cycle[4]. This chapter investigates the 3D printability and mechanical performance of recycled corn-based composites. The recycling process utilizes the gelatinization and retrogradation of starch molecules, requiring straightforward mechanical grinding and thermal activation of starch molecules with water. The recycled materials maintain their 3D printability and exhibit minimal changes in mechanical properties up to 5 recycling cycles. Furthermore, recycled composites demonstrate comparable mechanical performance to commonly used 3D printed thermoplastics and their composites, such as Polylactic acid (PLA) and PLA-wood fiber composites.

6.2 Materials and Methods: Before formulating the ink, 3D printed composites underwent

recycling by grinding using a 2.6 HP Table Type Ultra Fine Powder Pulverizing Machine (model RT-UF26). The resulting powdered composites were then mixed with water at 1800 rpm for 3 minutes using a Flacktek® DAC 400.2 VAC mixer. Subsequently, thermal treatments were conducted in a drying oven (manufactured by Huanghua Faithful Instrument Co., LTD) at 120°C for 10 minutes to induce gelatinization of amylopectin. Following heating, the resulting composite gels underwent mixing at 2000 rpm for 2 minutes followed by 1500 rpm for 2 minutes using the mixer. Rheological measurements, solidification of the 3D printed composites, and mechanical and microstructure characterizations were performed as described in sections 3.2.5-3.3.6, and 4.2.2-4.2.4, respectively. The recycling process of the 3D printed composites was repeated over 10 times using this methodology.

6.3 Results and discussion: Corn based composite materials are easy to recycle and require no chemical additives. Our approach focuses on breaking down the corn starch and cellulose fibers from the composite structure through grinding, followed by reformulating 3D printable ink through the thermal activation of starch molecules in the presence of water (Figure 6.1a). In the subsequent section, we will provide detailed discussion of how recycling affects the 3D printability of composite and their mechanical properties.

6.3.1 *Rheology of the recycled composite:* The rheological properties are crucial determinants of the printability of inks for Direct Ink Writing (DIW) processes. For printable materials, achieving shear thinning and yielding properties within an appropriate range of yield strength is essential. Rheological measurements, as depicted in Figure 6.1b-c, highlight the excellent printability of recycled corn-based composites. In Figure 6.1b, the shear-yielding behavior of both pristine and recycled composites is illustrated. Prior to the crossover point of the storage modulus (G') and loss modulus (G"), G' predominates over G", indicating a solid-like behavior. Subsequently, both

moduli exhibit a notable decrease, with the loss modulus surpassing the storage modulus beyond the crossover point, indicating a transition to fluid-like behavior during extrusion. Figure 6.1c depicts the shear-thinning behavior of the corn-based composites, where viscosity markedly decreases at higher shear rates. This characteristic facilitates smooth ink flow during extrusion, enhancing printability. Overall, the recycled composite demonstrates excellent 3D printability.

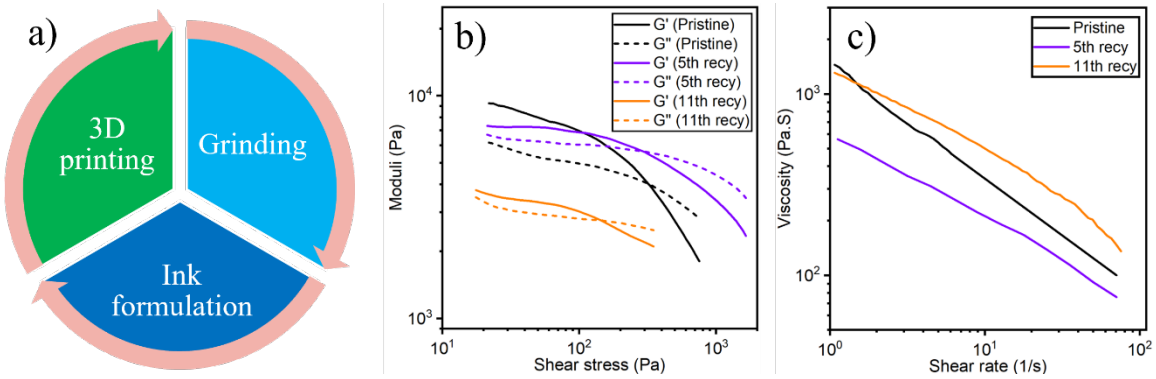

Figure 6.1: a) Recycling process for 3D printed corn composite. Rheology measurements of pristine and recycled corn-based composites. b) Shear yielding property and c) Shear thinning property.

6.3.2 *Mechanical properties of the recycled composite:* The assessment of mechanical properties is pivotal in assessing the impact of recyclability on composite materials. To investigate this, triangular cellular structures were 3D printed to examine how recycling frequency affects the mechanical robustness of the corn-based composite. These lightweight cellular structures were subjected to compression testing to quantify the effects of recycling on composite properties. Representative stress-strain curves derived from compression testing of both pristine and recycled composite specimens are depicted in Figure 6-2a. Figure 6-2b-d presents the results for specific strength, stiffness, and toughness for the recycled samples compared to the pristine specimen. Our experimental results indicate an increase in the stiffness of the recycled composite compared to the pristine specimens. For example, stiffness increased by 21.6% and 30% after the first and

seventh cycles, respectively. Although stiffness gradually decreased after the seventh recycling, overall recycled composites remained stiffer than their pristine counterparts. This stiffness enhancement is attributed to an increased fiber aspect ratio and enhanced fiber dispersion into the matrix resulting from repeated recycling and thermal treatment.

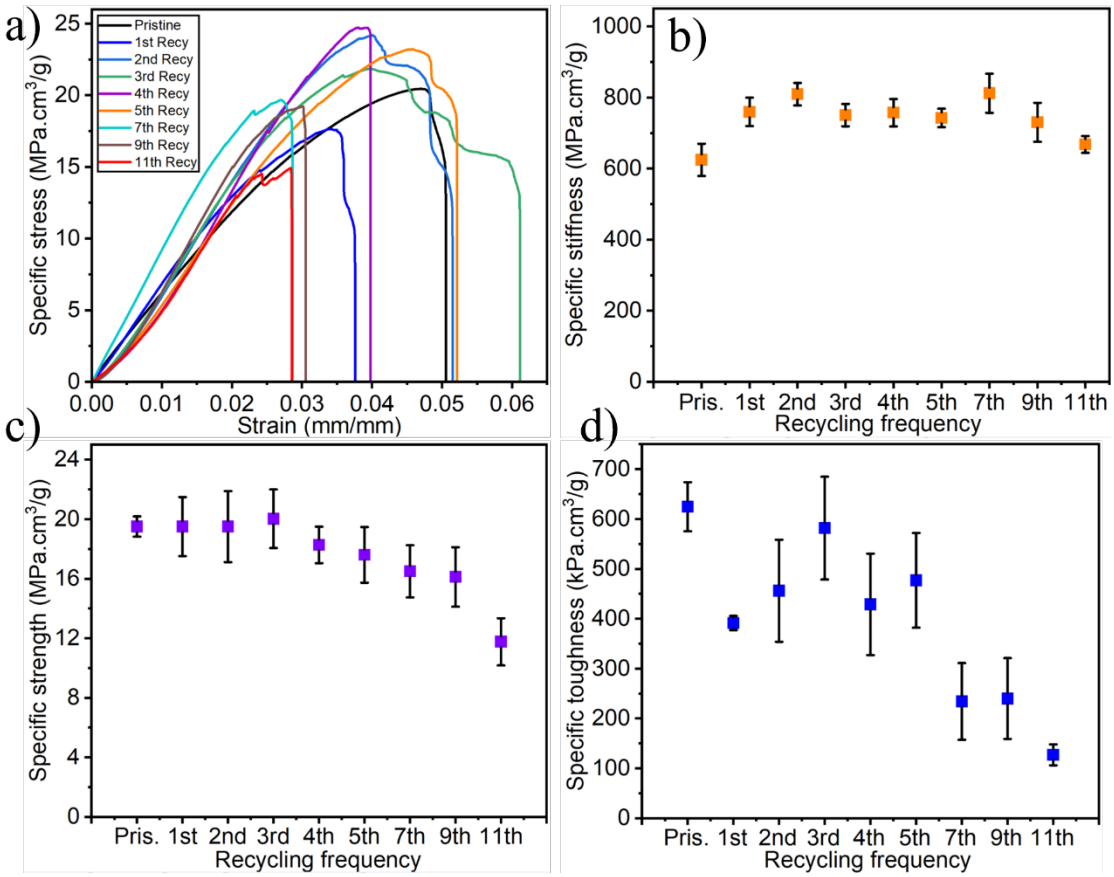

Figure 6.2: Mechanical properties of pristine and recycled composites. a) Stress-strain curves for composites with 10wt% cellulose fibers (CS-CF-10). b) Specific stiffness, c) strength and d) toughness of the CS-CF-10.

On the other hand, strength of the recycled composite remained comparable compared to the pristine samples in initial three generations (19.5 MPa·cm^3/g). However, beyond the third recycling, the specific strength of recycled composites began to linearly decrease, experiencing a total decrease of 39.6% after the 11th recycling. However, toughness of the recycled composites

consistently decreased with recycling frequency. The incorporation of cellulose fiber into the starch matrix typically enhances fracture toughness by promoting uniform load distribution and facilitating crack arrest and deflection. However, repeated recycling reduces cellulose fiber size, and smaller fillers fail to provide reinforcement to the composite, leading to a decrease in toughness with recycling frequency.

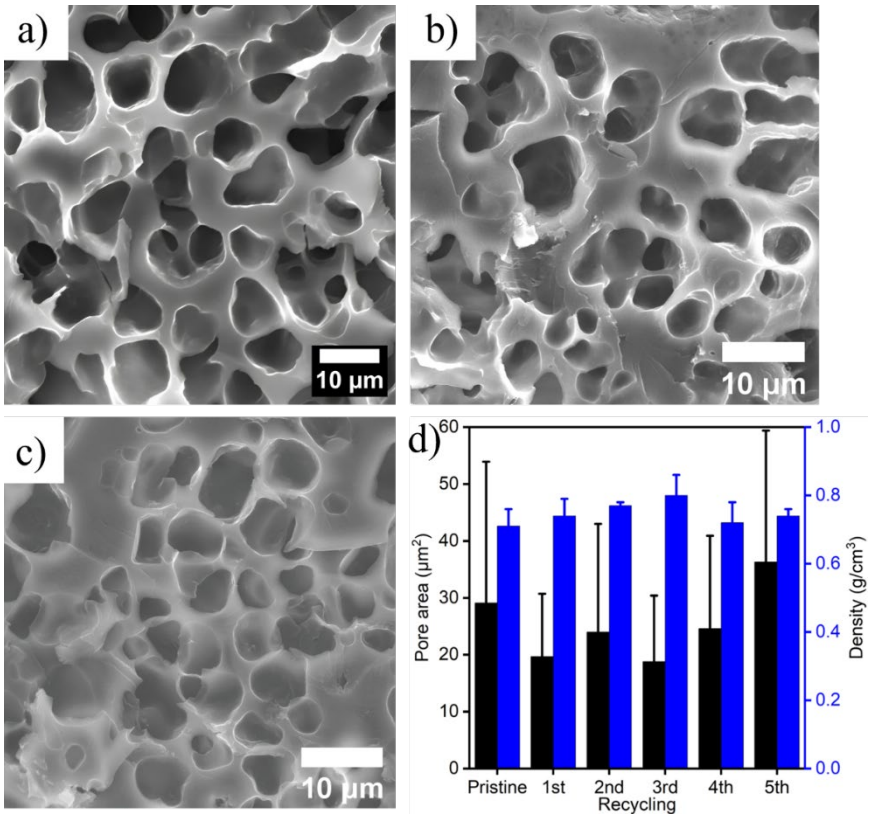

Figure 6.3: SEM images of the a) Pristine and recycled specimen after, b) 2nd and e) 4th recycle, d) Evaluation of micropore sizes and composite densities as a function of recycling frequency.

6.3.3 *Microstructure of the recycled composite:* Mechanical properties of composites are intricately linked with their microstructure. Hence, we conducted microstructural characterization to investigate the process-property-microstructure relationship for the recycled corn-based composite. The porous microstructures of the pristine and recycled samples are shown in the SEM images in Figure 6-3a-c. Pore size measurements showed that recycled specimens up to fourth

recycling exhibited smaller pores compared to pristine composites for comparable composite density (Figure 6-3d). This observation provides insight into the higher strength and stiffness observed in the recycled composites up to the fourth recycle.

6.3.4 Performance comparison: 3D printed corn composite vs commercial PLA-Wood composite: In the global 3D printing market, PLA-based materials are predominantly used, especially in FDM 3D printing. However, corn-based 3D printable composites have emerged as a promising alternative to address the extensive utilization of petroleum-based PLA plastics in 3D printing. To explore this further, we fabricated triangular cellular structures using PLA-Wood composite feedstock via FDM 3D printing. These structures were then subjected to compression testing, and their mechanical properties were compared with those of corn-based materials.

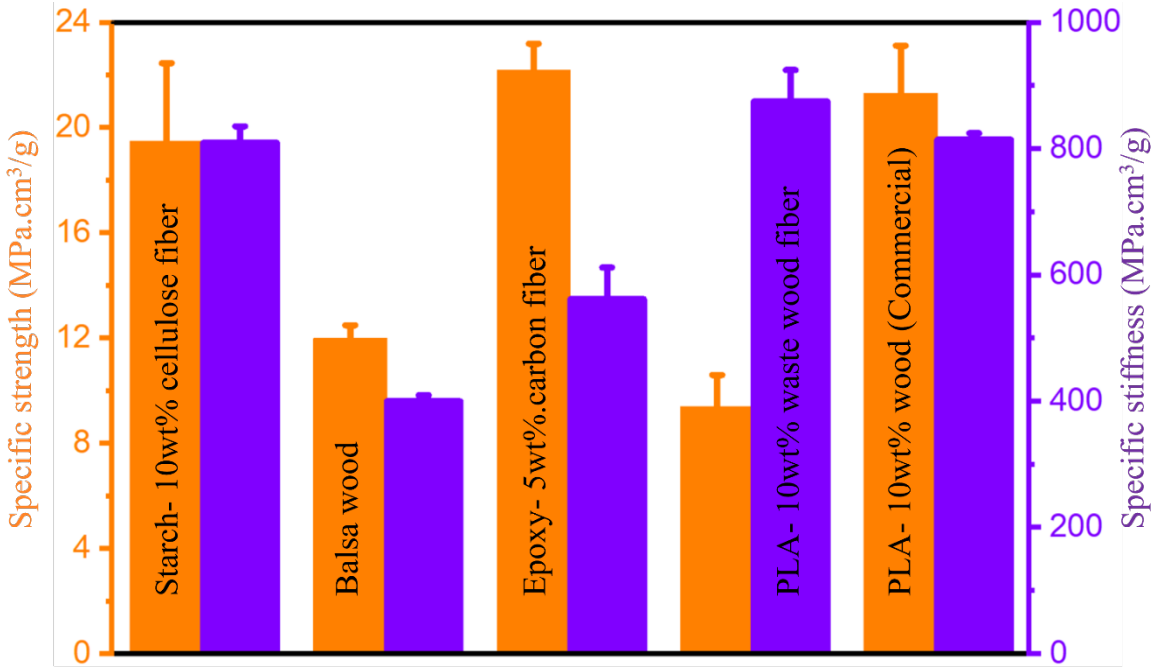

Figure 6.4: Mechanical properties of the balsa wood (perpendicular to grain), 3D printed starch-cellulose, epoxy-carbon fiber, PLA-waste wood, and commercial PLA-wood composite[17,26, 109].

Figure 6-4 presents a comparison of the mechanical properties for corn and PLA-Wood based composites. Our results indicate that the PLA-Wood composite exhibited strength and stiffness of 21.3 MPa and 814.6

MPa, respectively (Figure 6-7). Interestingly, the corn-based composite containing 10wt% of cellulose fibers displayed slightly lower strength and stiffness values of 19.5 MPa and 625 MPa, respectively (Figure 6-7). However, the corn-based composite containing 20wt% of cellulose fibers exhibited a comparable strength of 20.6 MPa and a 13% higher stiffness (920 MPa), respectively (Figure 6-7). These findings suggest a synergistic effect of using higher filler fraction into the starch matrix and the degree of amylopectin molecules gelatinization during the ink formulation process could further enhance the mechanical properties of the corn-based composite.

6.4 Chapter conclusion: In summary, we have presented a straightforward and chemical-free manufacturing route to produce mechanically robust and recyclable corn-based composites. Through mechanical grinding, we efficiently disintegrated corn starch and cellulose fibers from the composite structure after its service life, enabling the reformulation of 3D printable materials for direct ink writing additive manufacturing (AM) by leveraging thermal activation of amylopectin molecules in the presence of water. Rheological measurements highlighted the excellent 3D printability of the recycled composite compared to pristine composite. Moreover, our investigation into the process-property-microstructure relationships unveiled significant enhancements in material stiffness, reaching a maximum of 30% in the seventh recycle and a minimum of 7% in the eleventh recycle. This stiffness enhancement is attributed to an increased fiber aspect ratio and enhanced fiber dispersion into the matrix resulting from repeated recycling and thermal treatment. Our experimental findings indicate a comparable specific strength in the recycled composites compared to the pristine sample up to the third recycle. Despite initial promising results, we observed a consistent degradation in the strength of recycled composites, with a 39.6% decrease observed after the 11th recycling. This degradation is attributed to the filler effect, as repeated recycling leads to a reduction in cellulose fiber size, resulting in smaller fillers that fail to provide adequate reinforcement to the composite. Furthermore, compression testing

results demonstrated comparable strength in the 3D corn-based composite compared to commercial PLA-Wood composite, with a 13% higher stiffness observed for the corn-based composites. These findings support the potential of corn-based 3D printable composites as a promising alternative to petroleum-based PLA plastics in 3D printing technology, offering both environmental sustainability and mechanical performance benefits.

Chapter 7: Conclusions

In summary, I have developed sustainable and 3D printable composites exclusively from corn starch and cellulose fibers sourced from corn husks. By harnessing the unique gelatinization process in the amylopectin molecules and thermally activated interactions between amylopectin and cellulose fibers, I successfully achieved the desired ink rheology for 3D printing and tunable material properties across significant ranges for the printed composites. The process-structure-property relationships showed that, by using a preheating process, the microstructures could result in micropore sizes 26.6-62.5 μm^2 and material densities 0.48-0.75 g/cm^3. SEM images depicted distinct microstructural changes, while FTIR measurements clarified the formation of hydrogen bonds under various preheating conditions. Consequently, the mechanical properties were tunable within ranges of 2.5 to 3.3-fold in specific strength, stiffness, and toughness. Furthermore, I introduced a process-microstructure guided manufacturing approach for fabricating three-dimensional porous structures with hierarchical porosity. This methodology enables precise control over pore size at multiple length scales through the degree of gelatinization and 3D printing. The experimental results on the process-microstructure relationships showed that longer preheating treatments (14 minutes) at higher gelatinization temperatures (120°C) led to a notable reduction in micro pore area by over 2-fold and surface area of nanopores by over 3-fold. Moreover, these 3D printed corn-based composite materials are easily recyclable and demonstrate stable mechanical performance. This underscores their potential for displacing petroleum-based polymers and represents a significant step towards sustainable manufacturing practices. With the increasing demand for eco-friendly solutions, these corn-based composite materials present practical alternatives with diverse applications across advanced engineering and biomedical fields.

References

1. Rochman, C. M., Hoh, E., Hentschel, B. T. & Kaye, S. Classify plastic waste as hazardous. *Nature* **494**, 169–171 (2013).
2. Gibb, B. C. Plastics are forever. *Nat. Chem.* **11**, 394–395 (2019).
3. Bergmann, M., Tekman, M. B. & Gutow, L. Sea change for plastic pollution. *Nature* **544**, 297–297 (2017).
4. Mohanty, A. K., Vivekanandhan, S., Pin, J. M. & Misra, M. Composites from renewable and sustainable resources: Challenges and innovations. *Science (80-.).* **362**, 536–542 (2018).
5. UN Environmental Programme. *Drowning in Plastics – Marine Litter and Plastic Waste Vital Graphics*. 1–77 (2021).
6. Chamas, A. *et al.* Degradation Rates of Plastics in the Environment. *ACS Sustain. Chem. Eng.* **8**, 3494–3511 (2020).
7. Atiwesh, G., Mikhael, A., Parrish, C. C., Banoub, J. & Le, T.-A. T. Environmental impact of bioplastic use: A review. *Heliyon* **7**, E07918 (2021).
8. Xia, Q. *et al.* A strong, biodegradable and recyclable lignocellulosic bioplastic. *Nat. Sustain.* **4**, 627–635 (2021).
9. Lloyd, E. M. *et al.* Fully Recyclable Metastable Polymers and Composites. *Chem. Mater.* **31**, 398–406 (2019).
10. Guan, Q. F., Yang, H. Bin, Han, Z. M., Ling, Z. C. & Yu, S. H. An all-natural bioinspired structural material for plastic replacement. *Nat. Commun.* **11**, (2020).
11. Jiang, Y. & Raney, J. R. 3D Printing of Amylopectin-Based Natural Fiber Composites. *Adv. Mater. Technol.* **4**, 1900521 (2019).
12. Zhao, X. *et al.* Recycling of natural fiber composites: Challenges and opportunities. *Resour.*

Conserv. Recycl. **177**, 105962 (2022).

13. Xiao, S. *et al.* Lightweight, strong, moldable wood via cell wall engineering as a sustainable structural material. *Science (80-.).* **374**, 465–471 (2021).
14. Mohanty, A. K., Misra, M. & Hinrichsen, G. Biofibres, biodegradable polymers and biocomposites: An overview. *Macromol. Mater. Eng.* **276**–**277**, 1–24 (2000).
15. Rosenboom, J. G., Langer, R. & Traverso, G. Bioplastics for a circular economy. *Nat. Rev. Mater.* **7**, 117–137 (2022).
16. Song, J. *et al.* Processing bulk natural wood into a high-performance structural material. *Nature* **554**, 224–228 (2018).
17. Estakhrianhaghighi, E., Mirabolghasemi, A., Zhang, Y., Lessard, L. & Akbarzadeh, A. 3D-Printed Wood-Fiber Reinforced Architected Cellular Composites. *Adv. Eng. Mater.* **22**, 2000565 (2020).
18. Nguyen, N. A. *et al.* A path for lignin valorization via additive manufacturing of high-performance sustainable composites with enhanced 3D printability. *Sci. Adv.* **4**, eaat4967 (2018).
19. Pattinson, S. W. & Hart, A. J. Additive Manufacturing of Cellulosic Materials with Robust Mechanics and Antimicrobial Functionality. *Adv. Mater. Technol.* **2**, 1600084 (2017).
20. Sanandiya, N. D., Vijay, Y., Dimopoulou, M., Dritsas, S. & Fernandez, J. G. Large-scale additive manufacturing with bioinspired cellulosic materials. *Sci. Rep.* **8**, 8642 (2018).
21. Islam, M. N. & Jiang, Y. 3D Printable Sustainable Composites with Thermally Tunable Properties Entirely from Corn-Based Products. *ACS Sustain. Chem. Eng.* **10**, 7818–7824 (2022).
22. Khaled, S. A., Burley, J. C., Alexander, M. R. & Roberts, C. J. Desktop 3D printing of

controlled release pharmaceutical bilayer tablets. *Int. J. Pharm.* **461**, 105–111 (2014).

23. Siqueira, G. *et al.* Cellulose Nanocrystal Inks for 3D Printing of Textured Cellular Architectures. *Adv. Funct. Mater.* **27**, (2017).
24. Xu, W., Wang, X., Sandler, N., Willför, S. & Xu, C. Three-Dimensional Printing of Wood-Derived Biopolymers: A Review Focused on Biomedical Applications. *ACS Sustain. Chem. Eng.* **6**, 5663–5680 (2018).
25. Raney, J. R. *et al.* Rotational 3D printing of damage-tolerant composites with programmable mechanics. *Proc. Natl. Acad. Sci. U. S. A.* **115**, 1198–1203 (2018).
26. Compton, B. G. & Lewis, J. A. 3D-printing of lightweight cellular composites. *Adv. Mater.* **26**, 5930–5935 (2014).
27. Saadi, M. A. S. R. *et al.* Direct Ink Writing: A 3D Printing Technology for Diverse Materials. *Adv. Mater.* **34**, 2108855 (2022).
28. Lewis, J. A. Direct ink writing of 3D functional materials. *Adv. Funct. Mater.* **16**, 2193–2204 (2006).
29. Lam, C. X. F., Mo, X. M., Teoh, S. H. & Hutmacher, D. W. Scaffold development using 3D printing with a starch-based polymer. *Mater. Sci. Eng. C* **20**, 49–56 (2002).
30. USDA. *Grain : World Markets and Trade*. (2022).
31. *Corn in the U.S. - statistics & facts*. (2022).
32. Diyana, Z. N. *et al.* Physical properties of thermoplastic starch derived from natural resources and its blends: A review. *Polymers (Basel).* **13**, 1396 (2021).
33. Sakib, A.N., Bhuiyan, M.M.H., Corral, A.B. et al. Predictive modeling for mitigating fugitive emissions in industrial valve seal stacks: a comparative analysis of configuration efficacies. Neural Comput & Applic 36, 9263–9281 (2024).

34. Habib, A.K.M.A.; Sakib, A.N.; Mona, Z.T.; Bhuiyan, M.M.H.; Kazempoor, P.; Siddique, Z. Hydrogen-Assisted Aging Applied to Storage and Sealing Materials: A Comprehensive Review. Materials 2023, 16, 6689.

35. Jiang, T., Duan, Q., Zhu, J., Liu, H. & Yu, L. Starch-based biodegradable materials: Challenges and opportunities. *Adv. Ind. Eng. Polym. Res.* **3**, 8–18 (2020).

36. Zhou, Y., Fan, M. & Chen, L. Interface and bonding mechanisms of plant fibre composites: An overview. *Compos. Part B Eng.* **101**, 31–45 (2016).

37. Khaled, S. A., Burley, J. C., Alexander, M. R., Yang, J. & Roberts, C. J. 3D printing of tablets containing multiple drugs with defined release profiles. *Int. J. Pharm.* **494**, 643–650 (2015).

38. Khaled, S. A., Burley, J. C., Alexander, M. R., Yang, J. & Roberts, C. J. 3D printing of five-in-one dose combination polypill with defined immediate and sustained release profiles. *J. Control. Release* **217**, 308–314 (2015).

39. Xiang, H. *et al.* Green flexible electronics based on starch. *npj Flex. Electron.* **6**, 2022 (2022).

40. Bodkhe, S., Turcot, G., Gosselin, F. P. & Therriault, D. One-Step Solvent Evaporation-Assisted 3D Printing of Piezoelectric PVDF Nanocomposite Structures. *ACS Appl. Mater. Interfaces* **9**, 20833–20842 (2017).

41. Fu, K. *et al.* Graphene Oxide-Based Electrode Inks for 3D-Printed Lithium-Ion Batteries. *Adv. Mater.* **28**, 2587–2594 (2016).

42. Sun, K. *et al.* 3D printing of interdigitated Li-ion microbattery architectures. *Adv. Mater.* **25**, 4539–4543 (2013).

43. Sydney Gladman, A., Matsumoto, E. A., Nuzzo, R. G., Mahadevan, L. & Lewis, J. A. Biomimetic 4D printing. *Nat. Mater.* **15**, 413–418 (2016).

44. Rosen, D. W. Stereolithography and Rapid Prototyping. in *BioNanoFluidic MEMS* 175–196

(2008). doi:10.1007/978-0-387-46283-7_7

45. Ford, S. & Despeisse, M. Additive manufacturing and sustainability: an exploratory study of the advantages and challenges. *J. Clean. Prod.* **137**, 1573–1587 (2016).
46. Mani, M., Lyons, K. W. & Gupta, S. K. Sustainability characterization for additive manufacturing. *J. Res. Natl. Inst. Stand. Technol.* **119**, 419–428 (2014).
47. Ellis, J., Mavromatos, N. E., Nanopoulos, D. V. & Sakharov, A. S. Direct writing of three-dimensional webs. *Nature* **428**, 386 (2004).
48. Zhang, J. *et al.* 3D printed piezoelectric BNNTs nanocomposites with tunable interface and microarchitectures for self-powered conformal sensors. *Nano Energy* **77**, 105300 (2020).
49. Kumar, S. Selective Laser Sintering: A Qualitative and Objective Approach. *Jom* **55**, 43–47.
50. Khatri, N. R. *et al.* Integrating helicoid channels for passive control of fiber alignment in direct-write 3D printing. *Addit. Manuf.* **48**, 102419 (2021).
51. Skylar-Scott, M. A., Mueller, J., Visser, C. W. & Lewis, J. A. Voxelated soft matter via multimaterial multinozzle 3D printing. *Nature* **575**, 330–335 (2019).
52. Li, X. *et al.* Multimaterial Microfluidic 3D Printing of Textured Composites with Liquid Inclusions. *Adv. Sci.* **6**, 1800730 (2019).
53. Tang, Y., Dai, B., Su, B. & Shi, Y. Recent Advances of 4D Printing Technologies Toward Soft Tactile Sensors. *Front. Mater.* **8**, 658046 (2021).
54. Chen, S. *et al.* Engineering Natural Pollen Grains as Multifunctional 3D Printing Materials. *Adv. Funct. Mater.* **31**, 1–11 (2021).
55. Fan, T. F. *et al.* Transformation of hard pollen into soft matter. *Nat. Commun.* **11**, (2020).
56. Zhang, Y. *et al.* Photopolymerization of Pollen Based Biosourced Composites and Applications in 3D and 4D Printing. *Macromol. Mater. Eng.* **306**, 1–10 (2021).

57. Bakkal, M., Bodur, et al. The effect of reprocessing on the tensile properties of composites. *AIP Conf. Proc. 1315, 215–220 (2011).*

58. Bakkal, M., Bodur, M. S., Berkalp, O. B. & Yilmaz, S. The effect of reprocessing on the mechanical properties of the waste fabric reinforced composites. *J. Mater. Process. Technol.* **212**, 2541–2548 (2012).

59. Uitterhaegen, E. *et al.* Performance, durability and recycling of thermoplastic biocomposites reinforced with coriander straw. *Compos. Part A Appl. Sci. Manuf.* **113**, 254–263 (2018).

60. Lee, S. S., Santschi, M. & Ferguson, S. J. A Biomimetic Macroporous Hybrid Scaffold with Sustained Drug Delivery for Enhanced Bone Regeneration. *Biomacromolecules* **22**, 2460–2471 (2021).

61. Raeisdasteh Hokmabad, V., Davaran, S., Ramazani, A. & Salehi, R. Design and fabrication of porous biodegradable scaffolds: a strategy for tissue engineering. *J. Biomater. Sci. Polym. Ed.* **28**, 1797–1825 (2017).

62. Zhao, X. S. Novel porous materials for emerging applications. *J. Mater. Chem.* **16**, 623–625 (2006).

63. Hernandez, J. L. & Woodrow, K. A. Medical Applications of Porous Biomaterials: Features of Porosity and Tissue-Specific Implications for Biocompatibility. *Adv. Healthc. Mater.* **11**, 1–25 (2022).

64. Mohammadi, H., Sepantafar, M., Muhamad, N. & Bakar Sulong, A. How Does Scaffold Porosity Conduct Bone Tissue Regeneration? *Adv. Eng. Mater.* **23**, 1–19 (2021).

65. Dang, H. P., Shafiee, A., Lahr, C. A., Dargaville, T. R. & Tran, P. A. Local Doxorubicin Delivery via 3D-Printed Porous Scaffolds Reduces Systemic Cytotoxicity and Breast Cancer Recurrence in Mice. *Adv. Ther.* **3**, 1–14 (2020).

66. Edgar, K. J. & Marks, J. A. Green hydrogels based on starch: Preparation methods for biomedical applications. *ACS Symp. Ser.* **1372**, 173–196 (2020).

67. Tien, J. & Dance, Y. W. Microfluidic Biomaterials. *Adv. Healthc. Mater.* **10**, 1–16 (2021).

68. Dudukovic, N. A. *et al.* Cellular fluidics. *Nature* **595**, 58–65 (2021).

69. Mi, X. *et al.* Fabrication of highly porous starch monoliths and their application as green desiccants. *Polym. Adv. Technol.* **23**, 38–47 (2012).

70. Abbasi, N., Hamlet, S., Love, R. M. & Nguyen, N. T. Porous scaffolds for bone regeneration. *J. Sci. Adv. Mater. Devices* **5**, 1–9 (2020).

71. Thompson, B. R., Horozov, T. S., Stoyanov, S. D. & Paunov, V. N. Hierarchically structured composites and porous materials from soft templates: Fabrication and applications. *J. Mater. Chem. A* **7**, 8030–8049 (2019).

72. Corr, S. A., Shoemaker, D. P., Toberer, E. S. & Seshadri, R. Spontaneously formed porous and composite materials. *J. Mater. Chem.* **20**, 1413–1422 (2010).

73. Liu, M. C. *et al.* Three-Dimensional Interconnected Reticular Porous Carbon from Corn Starch by a Sample Sol-Gel Method Toward High-Performance Supercapacitors with Aqueous and Ionic Liquid Electrolytes. *ACS Sustain. Chem. Eng.* **7**, 18690–18699 (2019).

74. Yu, L. & Christie, G. Microstructure and mechanical properties of orientated thermoplastic starches. *J. Mater. Sci.* **40**, 111–116 (2005).

75. Liu, H., Yu, L., Xie, F. & Chen, L. Gelatinization of cornstarch with different amylose/amylopectin content. *Carbohydr. Polym.* **65**, 357–363 (2006).

76. Yan, L., Kasal, B. & Huang, L. A review of recent research on the use of cellulosic fibres, their fibre fabric reinforced cementitious, geo-polymer and polymer composites in civil engineering. *Compos. Part B Eng.* **92**, 94–132 (2016).

77. Nishimura, H., Kamiya, A., Nagata, T., Katahira, M. & Watanabe, T. Direct evidence for α ether linkage between lignin and carbohydrates in wood cell walls. *Sci. Rep.* **8**, 6538 (2018).

78. Terashima, N. *et al.* Nanostructural assembly of cellulose, hemicellulose, and lignin in the middle layer of secondary wall of ginkgo tracheid. *J. Wood Sci.* **55**, 409–416 (2009).

79. Börcsök, Z. & Pásztory, Z. The role of lignin in wood working processes using elevated temperatures: an abbreviated literature survey. *Eur. J. Wood Wood Prod.* **79**, 511–526 (2021).

80. Xu, J., Krietemeyer, E. F., Boddu, V. M., Liu, S. X. & Liu, W. C. Production and characterization of cellulose nanofibril (CNF) from agricultural waste corn stover. *Carbohydr. Polym.* **192**, 202–207 (2018).

81. Huda, S. & Yang, Y. Chemically extracted cornhusk fibers as reinforcement in light-weight poly(propylene) composites. *Macromol. Mater. Eng.* **293**, 235–243 (2008).

82. Song, J. *et al.* Processing bulk natural wood into a high-performance structural material. *Nature* **554**, 224–228 (2018).

83. Mazumdar, P., Chockalingam, S., Rattan, S. & Gupta, B. K. Tunable mechanical, electrical, and thermal properties of polymer nanocomposites through GMA bridging at interface. *ACS Omega* **3**, 3675–3687 (2018).

84. Broda, M., Curling, S. F. & Frankowski, M. The effect of the drying method on the cell wall structure and sorption properties of waterlogged archaeological wood. *Wood Sci. Technol.* **55**, 971–989 (2021).

85. Qian, L. & Zhang, H. Controlled freezing and freeze drying: A versatile route for porous and micro-/nano-structured materials. *J. Chem. Technol. Biotechnol.* **86**, 172–184 (2011).

86. Li, V. C. F., Dunn, C. K., Zhang, Z., Deng, Y. & Qi, H. J. Direct Ink Write (DIW) 3D Printed Cellulose Nanocrystal Aerogel Structures. *Sci. Rep.* **7**, 8018 (2017).

87. Oyinloye, T. M. & Yoon, W. B. Effect of freeze-drying on quality and grinding process of food produce: A review. *Processes* **8**, 354 (2020).

88. Kuo, C. C., Qin, H., Cheng, Y., Jiang, X. & Shi, X. An integrated manufacturing strategy to fabricate delivery system using gelatin/alginate hybrid hydrogels: 3D printing and freeze-drying. *Food Hydrocoll.* **111**, 106262 (2021).

89. Kubovský, I., Kačíková, D. & Kačík, F. Structural changes of oak wood main components caused by thermal modification. *Polymers (Basel).* **12**, 485 (2020).

90. Bajpai, P. Properties of biobased packaging material. in *Biobased Polymers* 25–111 (2019). doi:10.1016/b978-0-12-818404-2.00003-5

91. Affdl, J. C. H. & Kardos, J. L. The Halpin-Tsai equations: A review. *Polym. Eng. Sci.* **16**, 344–352 (1976).

92. Ghafaar, M. A., Mazen, A. A. & El-Mahallawy, N. A. Application of the Rule of Mixtures and Halpin-Tsai Equations To Woven Fabric Reinforced Epoxy Composites. *JES. J. Eng. Sci.* **34**, 227–236 (2006).

93. Sari, N. H., Wardana, I. N. G., Irawan, Y. S. & Siswanto, E. Physical and Acoustical Properties of Corn Husk Fiber Panels. *Adv. Acoust. Vib.* **2016**, 8 (2016).

94. Fleck, N. A., Deshpande, V. S. & Ashby, M. F. Micro-architectured materials: Past, present and future. *Proc. R. Soc. A Math. Phys. Eng. Sci.* **466**, 2495–2516 (2010).

95. Cantrell, J. H. Hydrogen bonds, interfacial stiffness moduli, and the interlaminar shear strength of carbon fiber-epoxy matrix composites. *AIP Adv.* **5**, 037125 (2015).

96. Huang, X., Nakagawa, S., Houjou, H. & Yoshie, N. Insights into the Role of Hydrogen Bonds on the Mechanical Properties of Polymer Networks. *Macromolecules* **54**, 4070–4080 (2021).

97. Provaggi, E., Capelli, C., Rahmani, B., Burriesci, G. & Kalaskar, D. M. 3D printing assisted

finite element analysis for optimising the manufacturing parameters of a lumbar fusion cage. *Mater. Des.* **163**, 107540 (2019).

98. Vargas-Alfredo, N., Dorronsoro, A., Cortajarena, A. L. & Rodríguez-Hernández, J. Antimicrobial 3D Porous Scaffolds Prepared by Additive Manufacturing and Breath Figures. *ACS Appl. Mater. Interfaces* **9**, 37454–37462 (2017).
99. Uziel, A., Shpigel, T., Goldin, N. & Lewitus, D. Y. Three-dimensional printing for drug delivery devices: a state-of-the-art survey. *J. 3D Print. Med.* **3**, 95–109 (2019).
100. *Yahoo! Finance: 3D Printing Filament Market* (2024) (Link).
101. *Forlab: Guide to Selective Laser Sintering (SLS) 3D Printings*. (Link).
102. S. Tagliaferri et al. Direct ink writing of energy materials. Mater. Adv., 2021,2, 540-563.
103. O. Sinitsky et al. The Mechanical Response of Epoxy–Sisal Composites Considering Fiber Anisotropy: A Computational and Experimental Study. Fibers 2022, 10(5), 43.
104. Chenrayan, V., Shahapurkar, K. et al. Experimental and numerical assessment of the flexural response of banana fiber sandwich epoxy composite. Sci Rep 13, 18156 (2023).
105. E. W. Gaba et al. The Influence of Pineapple Leaf Fiber Orientation and Volume Fraction on Methyl Methacrylate-Based Polymer Matrix for Prosthetic Socket Application.
106. Kenaf Fiber Industry: Investing Sneak Preview (Link)
107. Islam, M., Saito, J., Emdad, E. et al. Comparative genomics of two jute species and insight into fibre biogenesis. Nature Plants 3, 16223 (2017).
108. D. J. Hinchliffe et al. Multi-omics analysis of pigmentation related to proanthocyanidin biosynthesis in brown cotton (Gossypium hirsutum L.). Front. Plant Sci., 12 March, 2024.
109. Ben Wang, Yueke Ming et al. Fabrication of triangular corrugated structure using 3D printed continuous carbon fiber-reinforced thermosetting epoxy composites, Polymer Testing,

Volume 106, 2022, 107469